GCAGS JOURNAL
A Publication of the Gulf Coast Association of Geological Societies
www.gcags.org

VOLUME FRACTIONS OF LITHOLOGIC UNITS DEPOSITED PER GEOLOGIC EPOCH IN THE CENOZOIC, KEATHLEY CANYON AND WALKER RIDGE, DEEPWATER GULF OF MEXICO: PART 1—SAND, SHALE, AND SILTSTONE

Sharon Cornelius[1] and Peter A. Emmet[2]

[1]*Department of Earth and Atmospheric Sciences, University of Houston, Science and Research Bldg. 1, 3507 Cullen Blvd. #312, Houston, Texas 77204, U.S.A.*

[2]*Brazos Valley GeoServices, Inc., 19831 Cypress Church Rd., Cypress, Texas 77433, U.S.A.*

ABSTRACT

Borehole mudlog data from 80 wells in conjunction with 35 paleontological reports are used to define Cenozoic geological epochs within each borehole, both above and below the allochthonous salt canopy where salt is present. Isochore contour maps show how sediment depositional volumes vary within the study area on a per epoch (Paleocene, Eocene, Oligocene, Miocene, Pliocene, and Pleistocene) basis. The volume fractions of sandstone, shale, siltstone, limestone, and marl were also calculated by epoch, and contoured on a regional basis to understand the changes in the regional distribution of lithologies through time. These maps show how local deposition compares on a regional basis; and how depositional patterns change over the Cenozoic era. From the Paleocene to the Pleistocene, the volume fraction of sandstone in the study area has continuously decreased while during the same time period, the volume fraction of shale has increased. Sand volume fractions appear to have an inverse relationship with both shale and siltstone, meaning where there is a large volume fraction of sandstone present, the volume fraction of both shale and siltstone will be small. Volcanic tuff is present in fourteen wells, but there is insufficient data to map the regional distribution of volcanic tuff that is either Miocene, Oligocene, or Eocene in age according to the paleontological age of encasing sediments. In Part 1, the distribution and depositional histories of sandstone, shale and siltstone are discussed and in Part 2 the distribution and depositional history of Cenozoic limestone and marl is discussed.

INTRODUCTION

The main objective of this study was to contour the volume fraction (percentage) of sandstone, shale, siltstone, limestone, and marl over the study area by geological epoch to observe changes in depositional patterns over time. Sediment sourcing and depositional maps for Cenozoic stratigraphy in the western and central parts of the northern Gulf of Mexico usually have only broad lithologic generalizations for the lower slope regions approaching the Sigsbee Escarpment, due to lack of detailed well data at the time of their creation (Galloway et al., 2000; McDonnell et al., 2008). The drilling boom for Wilcox Group reservoirs in these deepwater provinces began around the year 2007 (Energy Information Administration [EIA], 2015). Part 1 of this study discussed here covers the distribution of sandstone, shale, and siltstone throughout the Cenozoic era within the study area. Part 2 (Cornelius and Emmet, 2018b, this volume) will cover the distribution of limestone and marl over Cenozoic geologic epochs in the same study area, along with an isochore contour map of the allochthonous salt derived from 93 of these area wells.

This work evolved from two previous geophysically-oriented studies in the same geographical area, using the same regional well log database. A geological 3D velocity model was created from high-resolution 2D seismic data and extensive well control (Cornelius and Emmet, 2018a). The velocity model in that study showed both high- and low-velocity anomalies within the allochthonous Louann Salt. The second study contains detailed analyses of these velocity variations within the salt, using mudlogs to determine the mineralogical content, showing that the velocity variations of the allochthonous salt that vary with latitude are due to variations in the salt mineralogy. Any effects caused by variation in temperature, pressure, or depth are insignificant (Cornelius and Castagna, 2018). This paper was in contrast to that of Fredrich et al. (2007), who concluded that mineralogical composition of allochthonous salt in the deepwater Gulf

Manuscript received February 5, 2018; revised manuscript received March 30, 2018; manuscript accepted May 17, 2018.

GCAGS Journal, v. 7 (2018), p. 121–150.

of Mexico was similar to the observed range of composition of salt domes located along the U.S. Gulf Coast. Fredrich et al. (2007)'s methodology was much better because he had actual salt cores; the problem is that ~90% of the wells used in the Cornelius study were drilled after 2006 (when the Fredrich et al. (2007) study was completed), so all the new well data significantly changed the perspective.

In this study, we use the same extensive well log database (276 digitized electric logs plus 108 mudlogs) in conjunction with all available Bureau of Ocean Energy Management (BOEM)–released paleontological and end-of-well reports (BOEM, 2018). The lithological contents of each borehole were subdivided into respective geologic epochs of the Cenozoic (Pleistocene, Pliocene, Miocene, Oligocene, Eocene, and Paleocene). The volume fractions of the various lithological components within each epoch were then calculated by using the lithological mudlogs for each borehole. Most boreholes contain allochthonous Louann Salt originally deposited in the Jurassic, which in its upward and seaward gravity gliding has modified the original stratigraphic column in many salt ascension zones and present-day welds (Moore et al., 1995; Hudec and Jackson, 2011). In addition, all allochthonous Gulf of Mexico (Gulf of Mexico) salt moves basinward over geologic time (Fort and Brun, 2012; Dribus et al., 2008), sometimes incorporating clastic sediment blocks from strata along its path. Only fourteen wells in the study area do not contain some amount of allochthonous salt.

A list of all individual wells mentioned in the text with their American Petroleum Institute–Unique Well Identifier (API–UWI) numbers is found in Table 1.

Study Area

The study area comprises all of Keathley Canyon and Walker Ridge protraction blocks, plus the southeastern corner of Green Canyon. Well control includes the Cobalt-operated Wilcox discovery well in Garden Banks block 959 #1, and the Anadarko operated Wilcox discovery well in Sigsbee Escarpment block 39 #1. The region was chosen because of industry interest over the past ten years, resulting in a large number of drilled wells with sufficiently robust borehole information to support the statistical validity of this study (Fig. 1).

Table 1. Wells mentioned in the text with their API–UWI designations.

Well name	API–UWI	Well name	API–UWI
GB–959–001–BP1	608074030502	KC–919–001	608084000600
GC–807–002	608114063500	KC–964–001	608084001400
KC–244–001–ST1	608084001201	WR–282–001	608124008600
KC–414–001	608084005000	WR–372–001	608124003000
KC–596–001	608084001300	WR–425–003–BP1	608124008100
KC–774–001	608084000300	WR–460–001	608124008400
KC–785–001	608084002100	WR–848–001	608124002600
KC–829–001–BP1	608084003101		

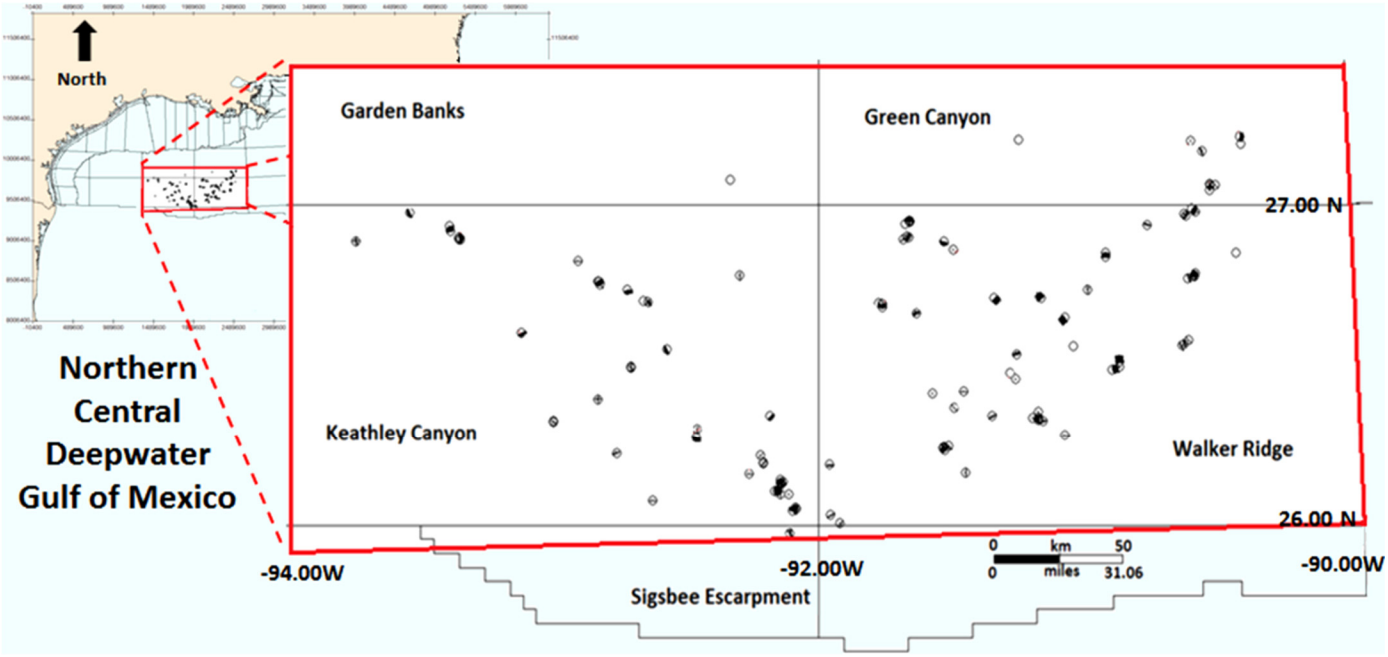

Figure 1. Deepwater Gulf of Mexico study area basemap showing all well locations used in this study. Open circles indicate vertical boreholes while other boreholes show the plan view of deviated drilling.

Database

There are eighty (80) wells within the study area having complete mudlog descriptions of the lithology within each borehole and 35 of 42 paleontological reports were considered to be usable for our purposes. A few of these BOEM–released paleontological reports cover only a portion of the well; and a few contain data from debris flows or overturned zones, where the strata are inverted. Reports for some wells contain microfossil data from salt-rafted or salt overturned zones, where the strata are inverted or otherwise out of place in the stratigraphic column. The database contains a total of 108 mudlogs, but some of these are redundant due to well sidetracks and well-bypass drilling. It is common for the lower part of these sidetracked or bypassed well zones to have different lithologies from that of the main borehole; i.e., lithology can noticeably change over short lateral distances in this deepwater region.

DETERMINATION OF GEOLOGICAL EPOCHS

Geological age of lithologic units (by epoch) was determined in two ways: (1) direct correlation of well log motif with a relevant biostratigraphic datum from a paleontological report; and/or (2) correlation of sequence boundaries and maximum flooding surfaces using a combination of gamma ray and resistivity electric logs. These paleontological reports were made by biostratigraphic contractors (chosen by each well operator) and usually are very detailed with a quantified list of all forams and nannofossils encountered in the borehole, such that last appearance datums are discernible. However, in some instances, the paleontological reports were not definitive, and by applying sequence stratigraphic methodology correlated with electric logs gave a more reliable answer. This means that determining the depth of a maximum flooding surface or a sequence boundary is more precise with a gamma ray log, and most Cenozoic epoch boundaries are determined by either a third-order maximum flooding surface or a sequence boundary.

Use of Paleontological Reports

In 33 of the 35 paleontological reports used in this study, the fossils present were sequential in age and provided straightforward epoch determination. The implication is that the limestone observed in 65 wells within the study area is truly Cenozoic in age where found below salt with other contemporaneous Cenozoic strata, as discussed in Part 2 (Cornelius and Emmet, 2018b, this volume). In this region we found borehole evidence of ten wells with rafted sections; but only four of them had confirming paleontological proof. Rafted sections are visible with seismic data; but no seismic data were used in the present study.

In a few locations, microfossils were stratigraphically out of place as noted by the presence of reworked fossils from older epochs. However, they were not the majority of all microfossils present, and consequently were ignored as out of place in the normal stratigraphic progression, possibly by faulting or salt movement. The occurrence of Miocene, Oligocene, and Eocene sediments both above and below the salt (both sets in biostratigraphic order) found in the borehole of the KC–470–001 well in Keathley Canyon, suggests that a sediment section became detached and subsequently was rafted on top of a salt diapir (Fiduk et al., 2014, 2016; Fiduk, 2017). The hypothesized salt structure is now a part of a larger salt canopy; but the rafted section is still attached. This is clearly documented by an abundance of definitive microfossils both above and below the salt. See Figure 2A for a schematic diagram of the mudlog for this well. In order to calculate the volume fractions on the individual components within each epoch, **only** Miocene B, Oligocene B, and Eocene B were considered as being representative of the insitu depositional units. Miocene A, Oligocene A, and Eocene A apparently were transported from elsewhere; therefore they are not representative of local depositional conditions at the borehole.

Another example of rafting occurs in the WR–969–001 well where a section of lower Paleogene strata, along with a section of upper-to-middle Cretaceous, has been rafted atop the present-day salt canopy (Fiduk et al., 2014, 2016; Fiduk, 2017) (Fig. 2B). Again, the rafted or out of place sedimentary components are not included in the estimated volume fractions of the normal stratigraphic sections below the salt.

In a few wells where salt was not very thick, such that there was a specific geologic epoch both above and below the salt, only interrupted by salt intrusion and not by rafting, those volumes were added together before calculating the component volume fractions. Generally speaking, where salt has displaced sediments from one or more geological epochs, the microfossils were reasonably sequential both above and below the salt. The biostratigraphic chart used to determine the geologic age of the individual microfossils found in the deepwater Gulf of Mexico is from Witrock (2017).

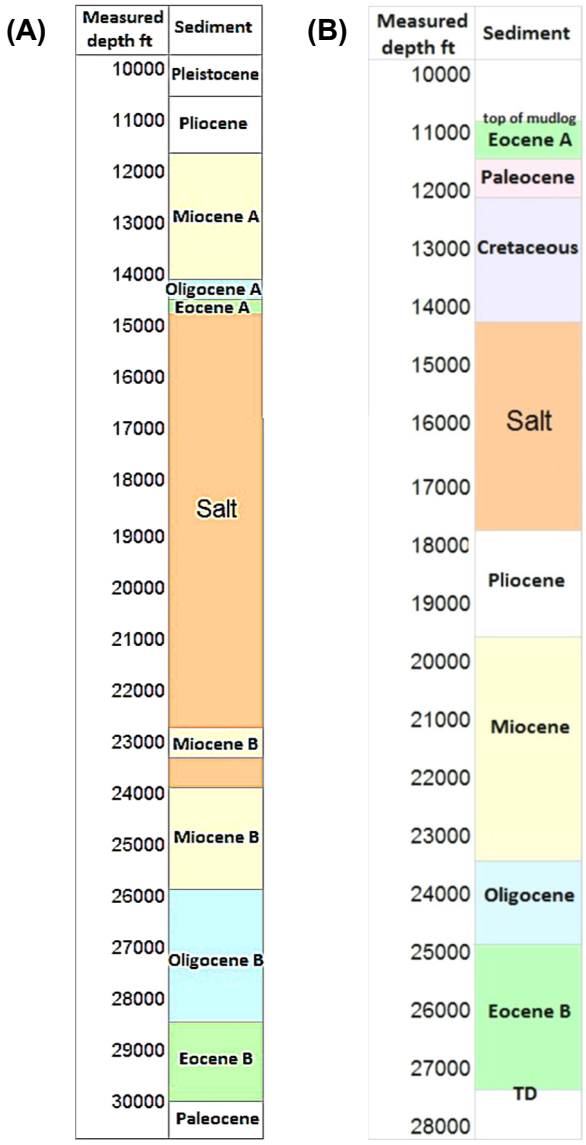

Figure 2. (A) Schematic diagram of ages for the KC–470–001 well showing rafted section above salt. (B) Schematic diagram of mudlog for the WR–969–001 well showing rafted section above salt.

Use of Well Log Sequence Stratigraphy

For the wells not having a paleontological report and not in proximity to a well that does, the alternative for defining geological age was to apply sequence stratigraphic principles. Two different sea-level charts were used as references: the 2005 version for global sea-level changes in the Cenozoic by Miller et al. (2005) (Fig. 3) and the 2000 version by Galloway et al. (2000) for sea-level changes in the Gulf of Mexico during the Cenozoic. Geological age transitions occur either at maximum flooding during sea-level rise or at sequence boundaries at the base of major sea-level falls (regressions). These defining stratigraphic surfaces are sometimes more recognizable on well logs than the transition zone of microfossils, which may occur over several hundred feet in the borehole.

Adjustment for Allochthonous Salt Presence

The salt presence in the borehole was ignored in the usual case of the stratigraphic column being sequential both above and

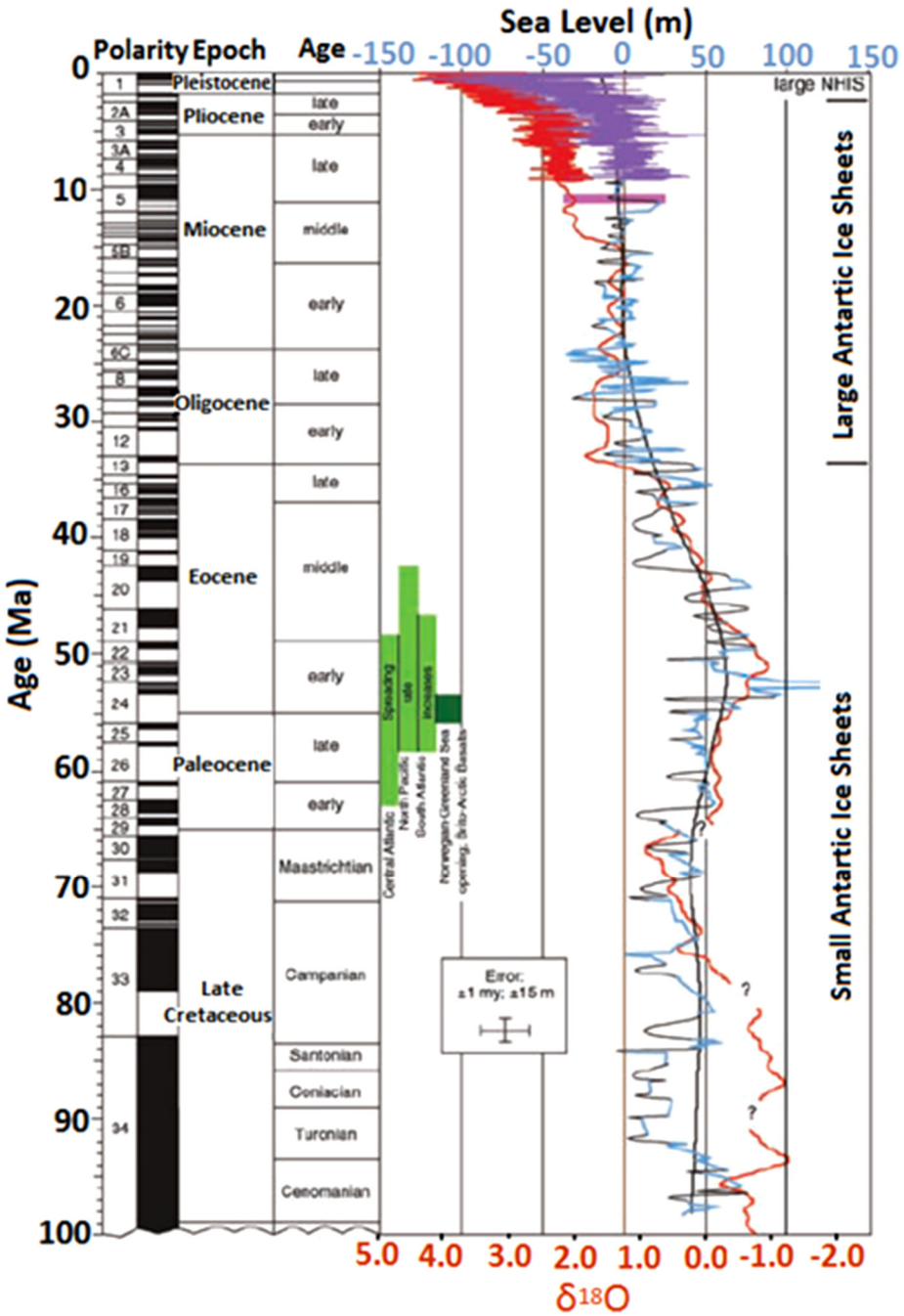

Figure 3. Global sea-level chart (modified after Miller et al., 2005). Sea level in blue for the interval 7 to 100 Ma is derived by backstripping data. Global sea level in purple for 0 to 7 Ma is derived from the $\delta^{18}O$. Shown for comparison is a benthic foraminiferal $\delta^{18}O$ from 0 to 100 Ma in red, with the scale on the bottom axis in per mille (‰). The pink box at the boundary between middle and late Miocene is a sea level estimate derived from the Marion Plateau. The heavy black line is the long term fit to our back-stripped curve. Light green boxes indicate times of spreading rate increase on various ocean ridges. Dark green box indicates the opening of the Norwegian-Greenland Sea.

below the salt. In the instance where salt occurred twice in the same borehole, the interim sediment had to be determined as to whether it belonged to the borehole stratigraphic column, or if it had been welded to the salt during the salt's continuous movement. The best analysis of the true stratigraphic column was found in the wells not having salt. These few wells demonstrated what the stratigraphic sequences would look like if not interrupted by salt. Of course, the present stratigraphy is a function of locale, topographic lows or highs, contemporaneous or subsequent faulting, and sediment sourcing rates from sediment sources migrating from west to east.

Cenozoic Sedimentation Rates for Clastics Deposited into the Gulf of Mexico Basin

There is much information in the literature regarding this topic; but the sources chosen for reference here come from Galloway et al. (2011) (Fig. 4) and Fort and Brun, (2012) (Fig. 5). The chart in Figure 4 summarizes the data in a compact format, showing the relative amounts of grain volume deposited per million years (divided by 1000) over the Cenozoic time span. The highest rates of sediment flow into the Gulf of Mexico Basin occurred for the Lower Wilcox sands during the Paleocene, and also for Pleistocene sands. However, Figure 5 shows the same overall trend for the Paleogene with high sediment supply during the Lower Paleocene, decreasing in the Upper Paleocene, continuing into the Eocene, but increasing again in the Lower Oligocene (Fort and Brun, 2012).

Equally important as the volume of sediment being deposited into the Gulf of Mexico Basin is the location of the depocenters over Cenozoic time (Fig. 6). We can see how these depocenters gradually shifted from west to east and progressively extended basinward from north to south (Dribus et al., 2008). The isochore map of the Pleistocene (Fig. 7) does show the thickest sedimentary units of any epoch within the study area, in support of Figures 4 and 5. Unfortunately, for the Paleocene data, there are only 32 wells within the study area that have drilled into the Paleocene; so we are missing much useful information. Recently

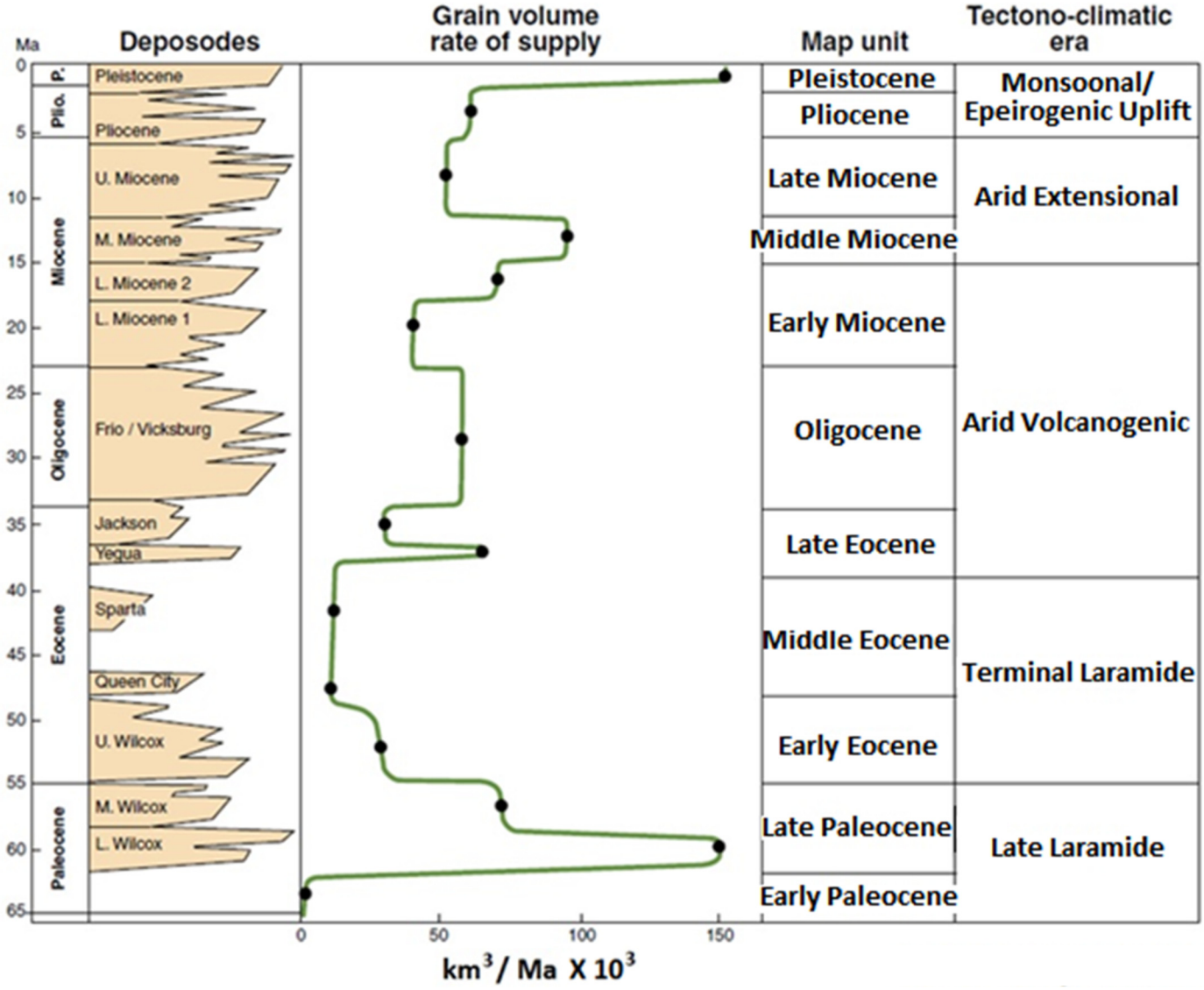

Figure 4. Relative rate of siliciclastic sediment supply to the Gulf of Mexico Basin during the Cenozoic (modified after Galloway et al., 2011). The grain volume column from this study indicates the relative sediment supply input into the Gulf of Mexico, but because there is no reference to grain size, it does not give any indication as to how far into the basin these grain volumes were distributed.

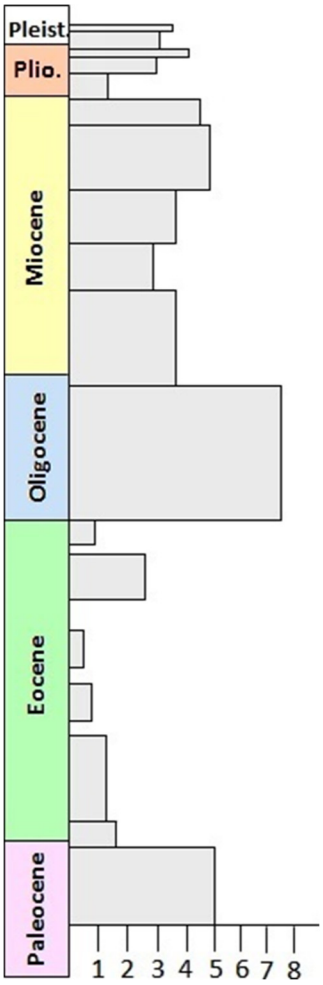

Figure 5. Input sedimentation rate in units of 10^4 km^3 per Ma for the northern Gulf of Mexico (modified after Fort and Brun, 2012). 1x10^4 km^3 = ~0.24x10^4 mi^3.

acquired well data from the Bureau of Safety and Environmental Enforcement (BSEE) (BSSE, 2018b) adds five more wells to the list of those penetrating the Paleocene, but they have not yet been analyzed for this study.

CALCULATION OF VOLUME FRACTIONS

Once every well had been subdivided into the geological epochs for that particular borehole, mudlogs were utilized to define lithologic percentages present within each epoch. There are a variety of lithologic categories, depending on well location and the level of detail unique to each contractor providing the mudlogs. For example, one meticulous contractor reported the presence of argillaceous shale, calcareous claystone, and shale in eleven of the wells, while other contractors just lumped these components (if present) together as "shale." These two constituents were not contoured due to insufficient data.

Three things to consider when viewing the volume fraction contour maps: (1) not all wells were drilled to the same depth; (2) the present-day water depths vary from 3956 ft (1206 m) to 9576 ft (2919 m), which may bear little relationship to the water depth at time of deposition; and (3) salt may have displaced one or more chronostratigraphic units in most locations. We feel that it is important to look at these maps as a reflection of what is actually in the well, which presents a more detailed representation of lithology than what a seismically-derived map would show. Admittedly, seismically-derived maps give better continuity than those from scattered well control; but then how do you verify the lithology you think is present in the seismic data? One important insight learned from analyzing these regional mudlogs is lateral variation in lithology over short distances, regardless of orientation along strike or along dip, these lithological changes are not likely visible on seismic data, especially below the salt canopy where the dominant seismic frequencies are less than 20 Hz.

GEOLOGICAL EPOCH ISOCHORE MAPS

This study utilized the IHS Markit Kingdom 2017 software application. We loaded the geological ages from each borehole into Kingdom to create "zones," defined by the top and base of each epoch in each well. This allowed us to generate an isochore (true vertical thickness) map for each epoch on a regional basis. These isochore maps, with thickness in feet, are shown in Figure 7 (Pleistocene), Figure 8 (Pliocene), Figure 9 (Miocene), Figure 10 (Oligocene), Figure 11 (Eocene), and Figure 12 (Paleocene). The isochore maps were made using flex gridding with minimal smoothing on an 8000 ft by 8000 ft (2438 m by 2438 m) grid using a 200,000 ft (~61,000 m) search radius.

Calculated volume fractions of the lithology as "zone attributes" were distributed into each previously defined "zone." We defined our attributes as % sandstone, % shale, % siltstone, % limestone, and % marl, which are the most common components for each epoch, only in different proportions. A few wells described the additional components of % argillaceous shale and % calcareous claystone, but only eleven wells reported this level of detail, so there were insufficient data points to map. Comparison among epochs shows that the Miocene had the thickest depositional units (Fig. 9) and the Paleocene (Fig. 12), the thinnest. The Eocene depositional thickness (Fig. 11) was almost twice that of the Paleocene, but this thickness diminished by 20% during the Oligocene (Fig. 10) due to a diminished supply of sand and silt. Pleistocene (Fig. 7) and Pliocene (Fig. 8) depositional thicknesses are similar and only 10% less than the Miocene.

VOLUME FRACTION CONTOUR MAPS

The lithologic maps we discuss in Part 1 (this paper) are those for sandstone, shale, and the siltstone. It is informative to compare the distribution of lithological constituents in the study area throughout the Cenozoic. It should be realized that volume fractions represent the relative amounts of lithologies deposited per geological epoch, and these are probably more accurately represented for the Eocene and the Paleocene epochs, which did not experience as much salt deformation as younger stratigraphic sections. Whole or partial sections of Pleistocene, Pliocene, Miocene, and/or Oligocene strata are missing in many boreholes due to salt tectonics. Some wells do not penetrate deeper than Pliocene or Miocene strata, so there is no data in those wells for the Oligocene, the Eocene, or the Paleocene. Only 51 wells penetrate the Eocene, and only 32 wells penetrate the Paleocene. The Oligocene has the highest number of well penetrations with 57 well data points. The number of well penetrations for these three epochs will increase with the addition of nine new wells waiting to be analyzed.

Cenozoic Sand Distribution in the Study Area

Sandstone distributions are considered first, as these are the primary reservoirs in the paleo-slope to deepwater paleoenvironments of the study area (Figs. 13–25). Sandstone maps are shown in Figure 13 (Paleocene), Figure 16 (Eocene), Figure 18 (Oligocene), Figure 20 (Miocene), Figure 22 (Pliocene), and in Figure 24 (Pleistocene). These are presented from "oldest" to "youngest," to best understand the temporal progression of depo-

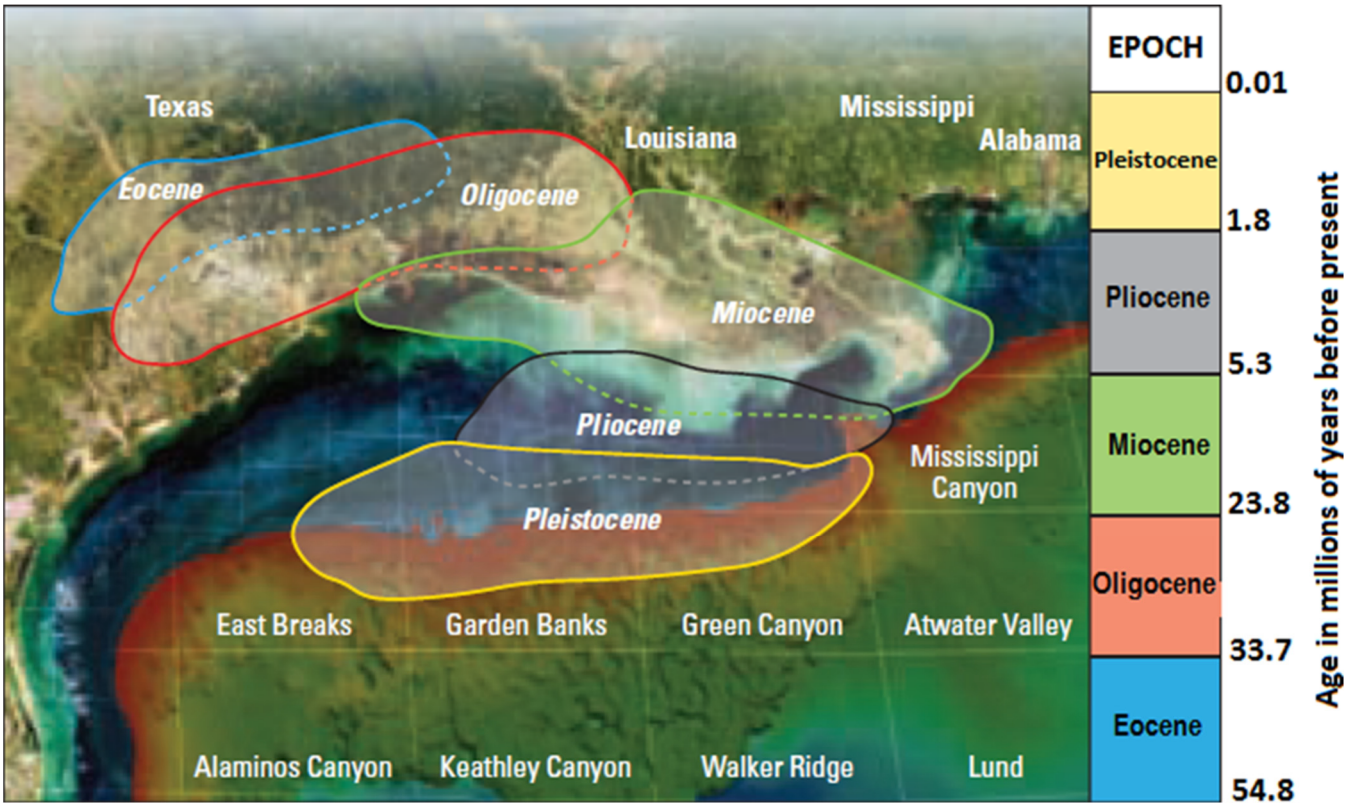

Figure 6. Cenozoic depocenters over time for the northern Gulf of Mexico Basin, shifting west to east and extending basinward from north to south (modified after Dribus et al., 2008).

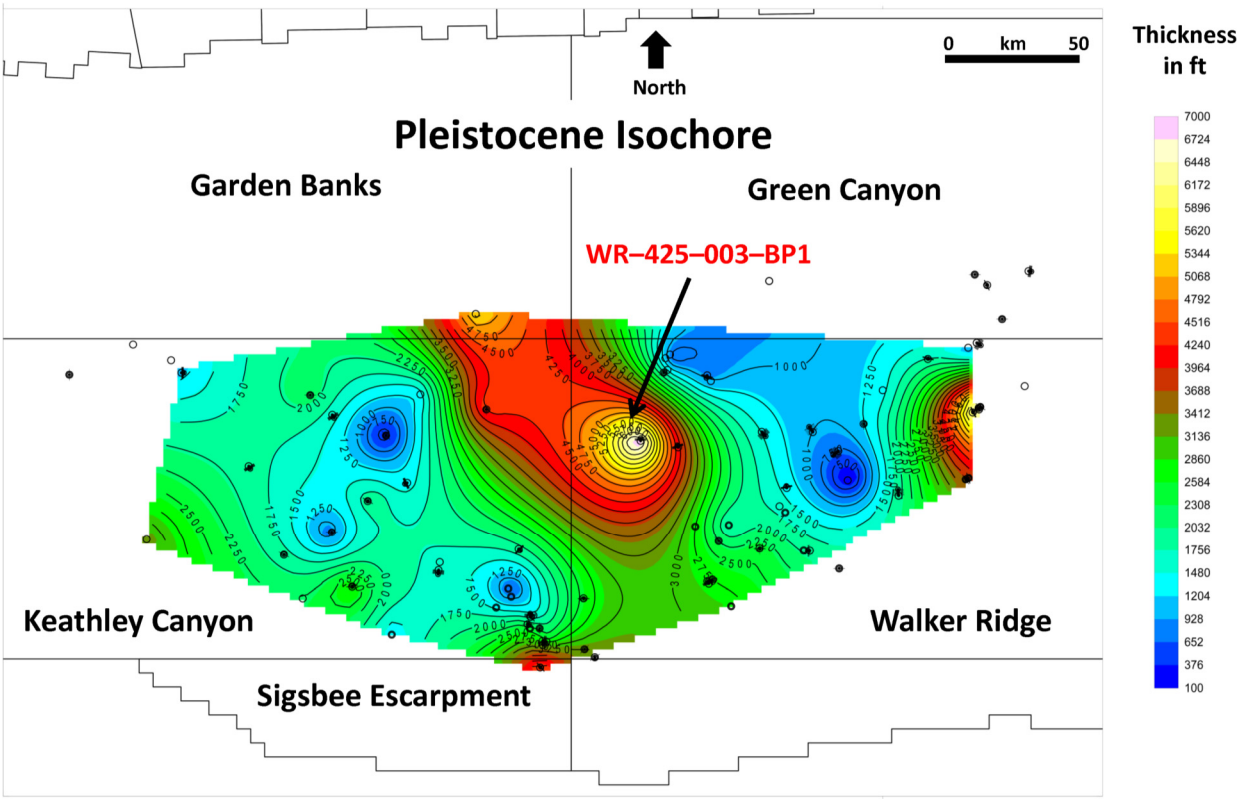

Figure 7. Isochore map of Pleistocene deposition. The thickest Pleistocene deposition in this map area was centered on the WR–425–003–BP1 well. 50 km = ~31 mi.

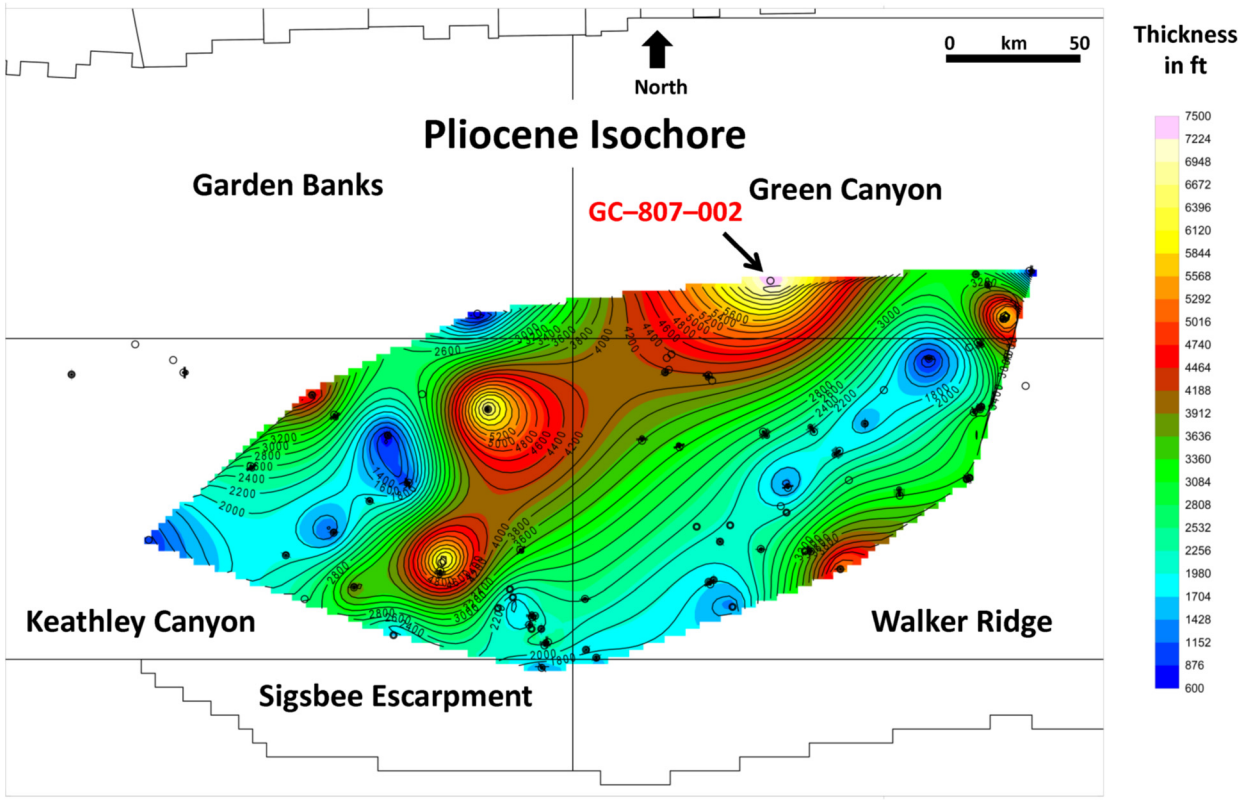

Figure 8. Isochore map of Pliocene deposition. The thickest Pliocene deposition in this map area was centered on the GC–807–002 well. Note that the depositional trend axis is perpendicular to the one in the Pleistocene shown in Figure 7. 50 km = ~31 mi.

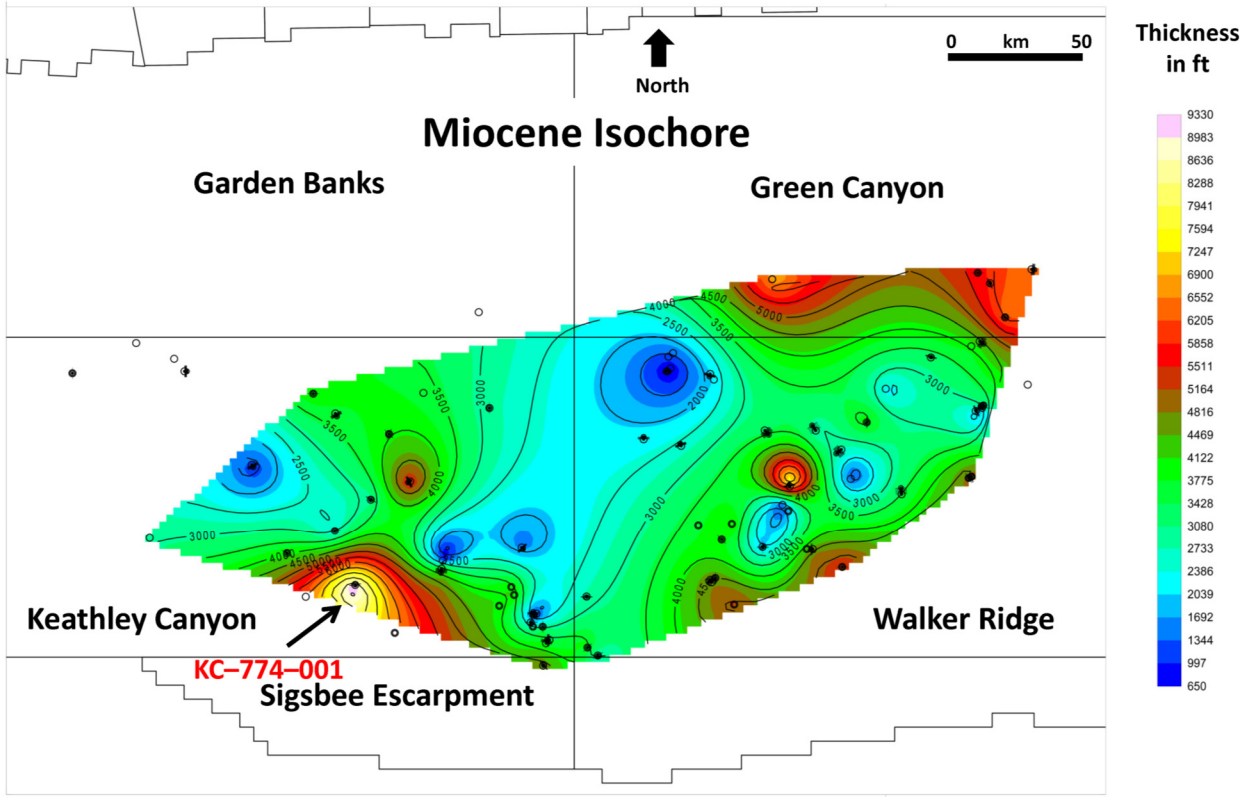

Figure 9. Isochore map of Miocene deposition. The thickest Miocene deposition in this map area was centered on the KC–774–001 well. 50 km = ~31 mi.

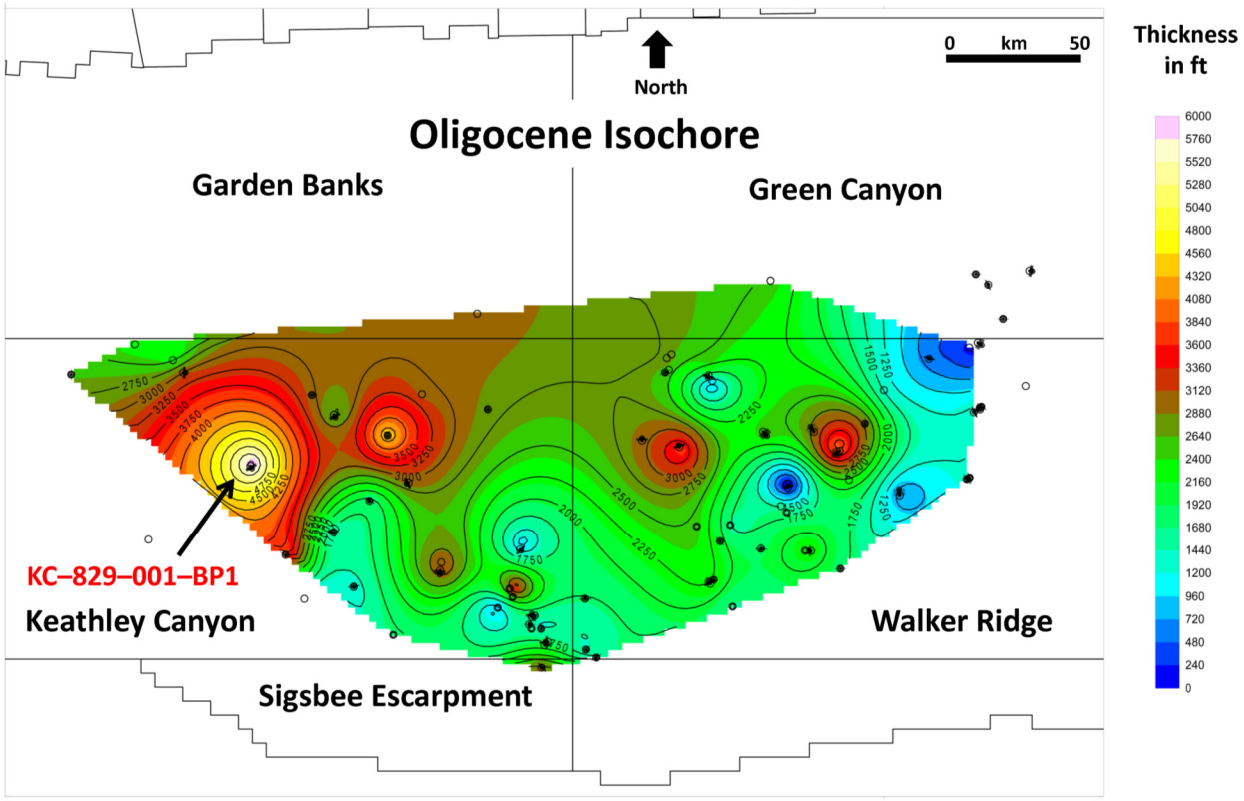

Figure 10. Isochore map of Oligocene deposition. The thickest Oligocene deposition in this map area was centered on the KC–829–001–BP1 well. 50 km = ~31 mi.

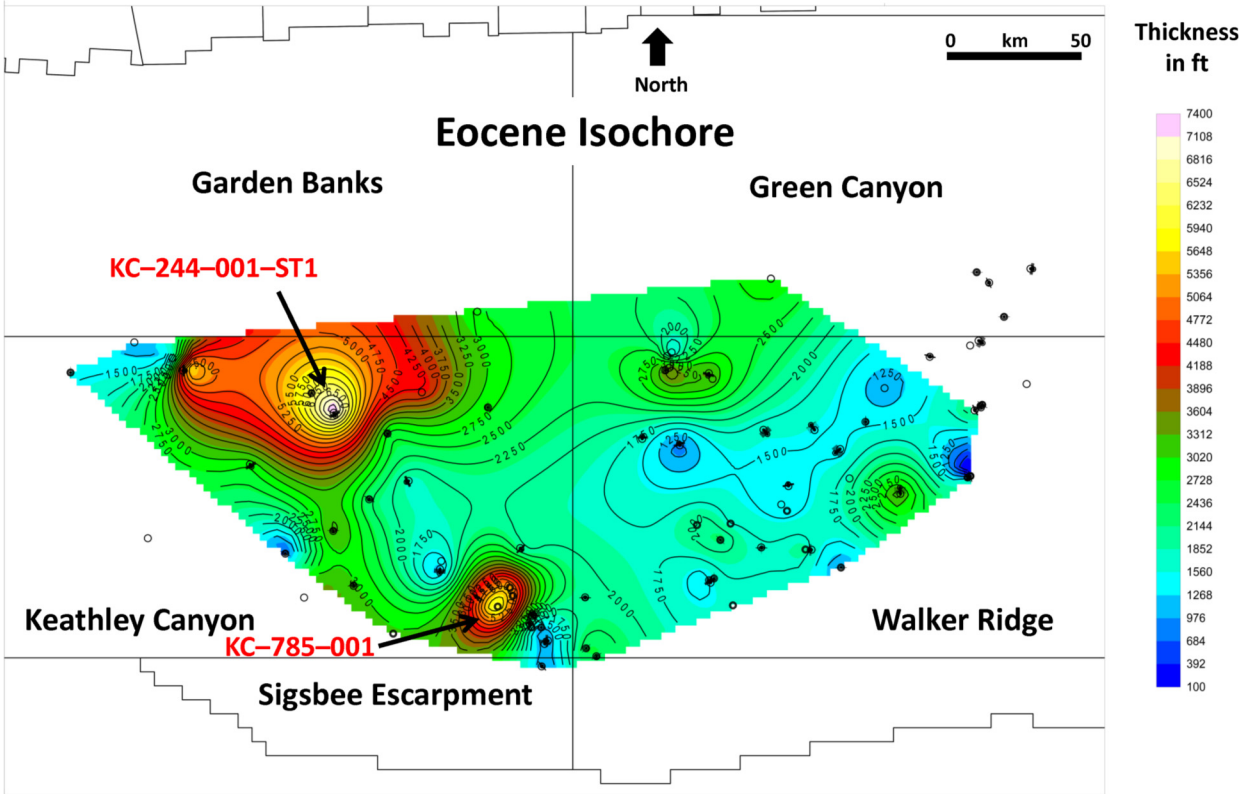

Figure 11. Isochore map of Eocene deposition. The thickest Eocene deposition in this map area is centered on the KC–244–001–ST1 well and the second thickest is centered on the KC–785–001 well. Note the isochore thickness in Keathley Canyon compared to relative lack thereof in Walker Ridge. During the Eocene the sediment source was to the northwest, so this depositional preference in location is expected. 50 km = ~31 mi.

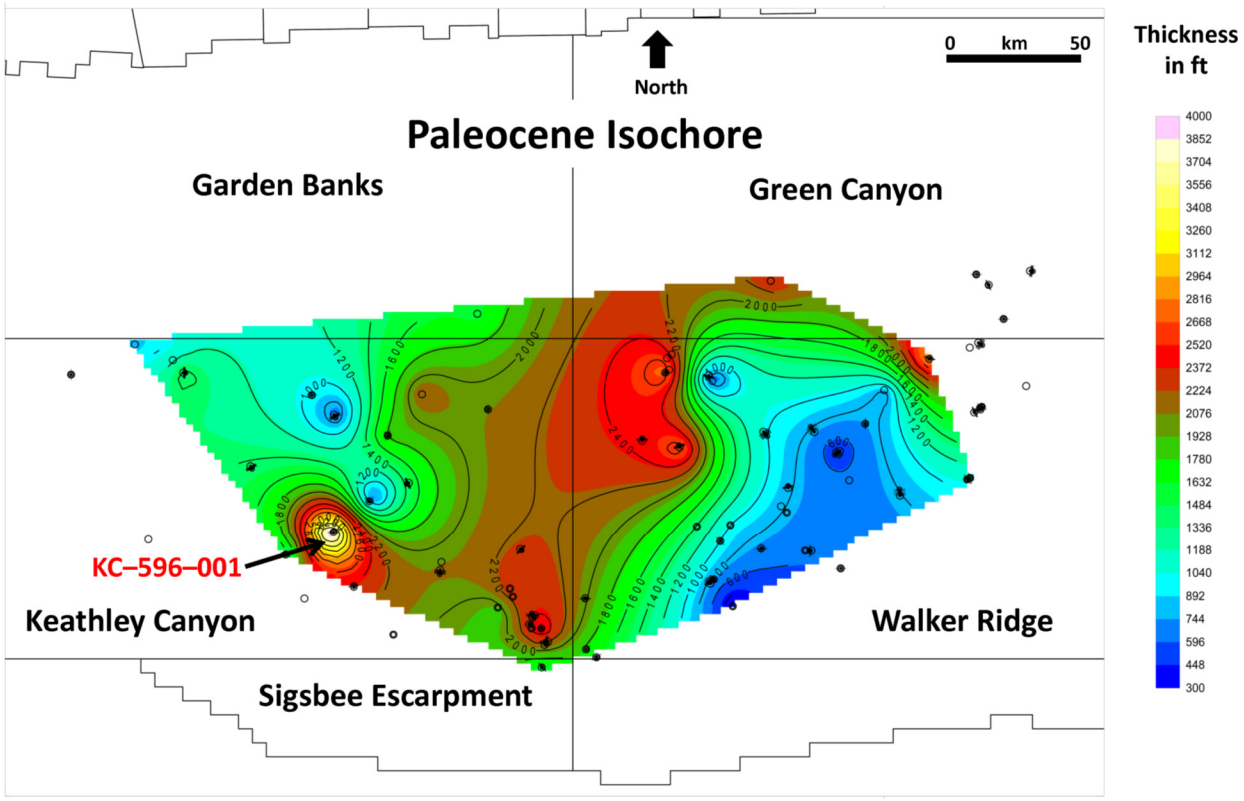

Figure 12. Isochore map of Paleocene deposition. The thickest Paleocene deposition in this map area is centered on the KC–596–001 well. 50 km = ~31 mi.

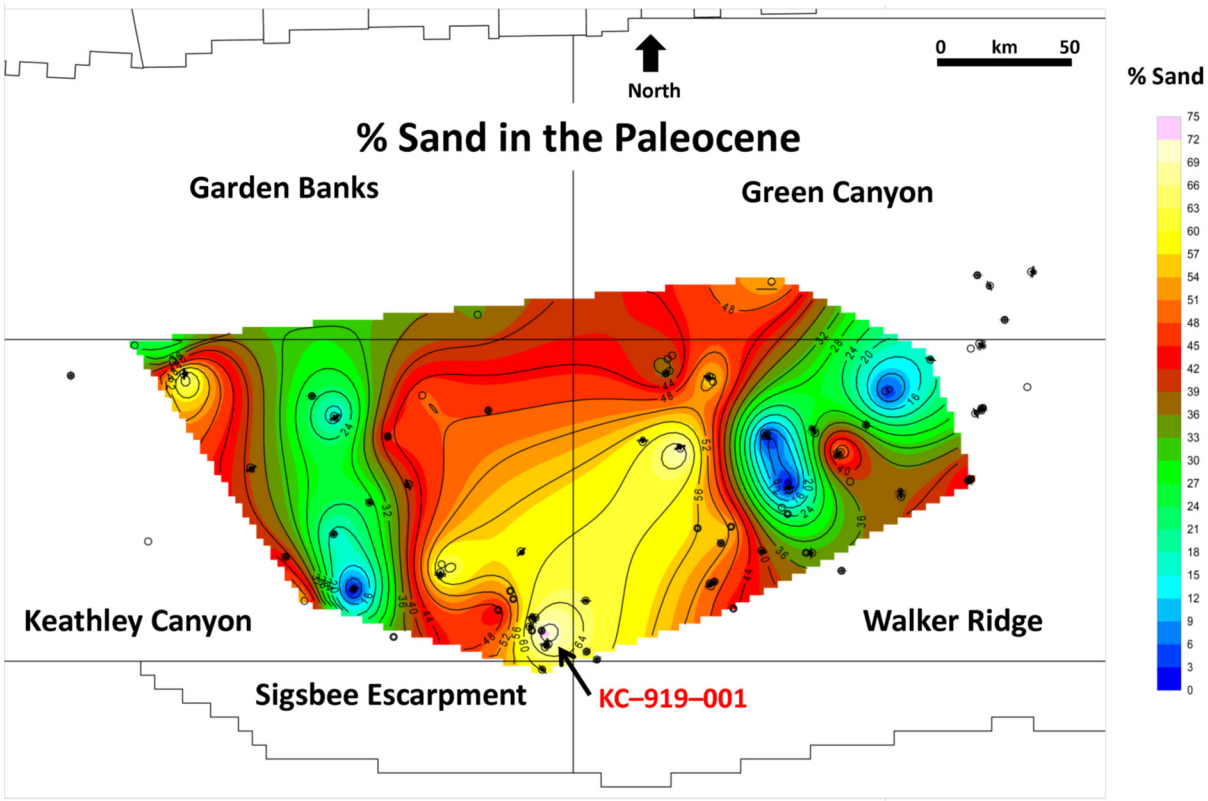

Figure 13. Map of percent (volume fraction) sandstone deposited during the Paleocene Epoch. The highest volume fraction of Paleocene sandstone is found in the KC–919–001 well. 50 km = ~31 mi.

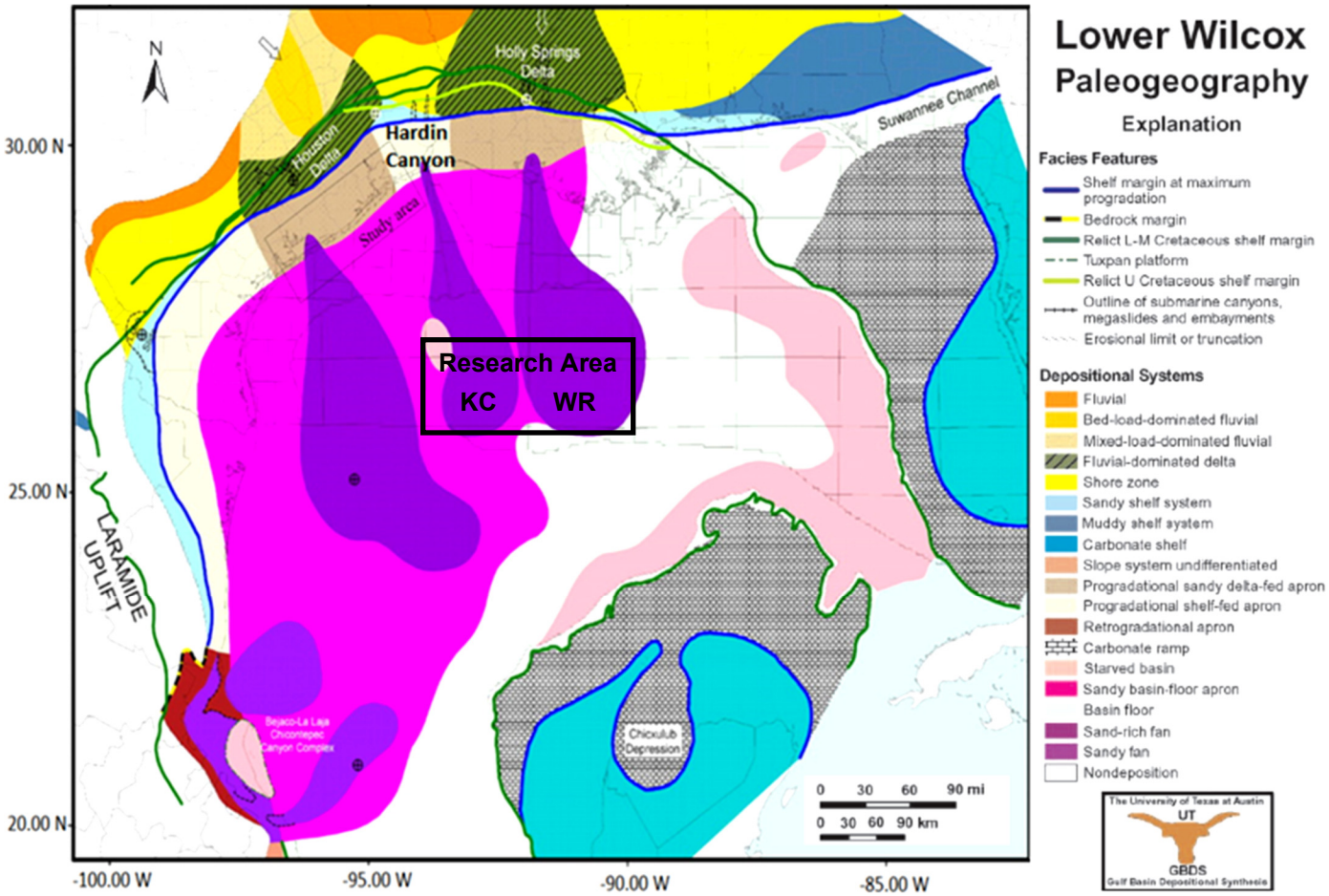

Figure 14. Paleocene sediment sourcing for Lower Wilcox sands in the deepwater Gulf of Mexico (modified after McDonnell et al., 2008). The dark purple units represent sandy slope to abyssal-plain fans and the magenta unit indicates a sand-rich basin floor aprons. The approximate study area is denoted by black-outlined box in the KC (Keathley Canyon) and WR (Walker Ridge) protraction areas.

sition in the study area. It is well documented that Cenozoic depocenters shifted eastward in the Gulf of Mexico over the Cenozoic Era (Galloway, 2008).

Paleocene Sandstone

A pronounced depositional axis of thick Paleocene sands trends southwest to northeast is seen in Figure 13. Since the Lower Wilcox was sourced primarily from the west to northwest during the Paleocene (Galloway et al., 2000, 2011; Rains et al., 2007; Zhang et al., 2017), one might have expected the depositional axis to more or less trend from southeast to the northwest. However, there is a subtle hint of a sandstone thickness trend developing along the western edge of the data. Limited well penetrations in the western part of Keathley Canyon likely affect the contouring. The Paleocene coastal plain to the uppermost continental slope succession of the Lower Wilcox shelf-margin prism is divided into eighteen high-frequency (~300 ky duration) stratigraphic sequences. Two outstanding characteristics of the Lower Wilcox system that help explain sediment delivery so distant from the shelf-edge into the deepwater Gulf of Mexico Basin are: (1) an unusually high sediment supply rate (>10 km/Ma [~6.1 mi/Ma] from major river systems); and (2) limited accommodation space on the shelf (Zhang et al., 2017). An important conclusion regarding the Lower Wilcox is that the depositional thickness tends to decrease from west to east (from Alaminos Canyon to Keathley Canyon to Walker Ridge to Atwater Valley [Fulthorpe et al., 2014], as supported by Figure 12), while at the same time, sandstone grain size also decreases from west to east. Within each slope fan complex, channel fill deposits exhibit the best reservoir quality because they contain a higher ratio of coarser-grained sandstone to siltstone, and thus higher permeability. The lobe margin sandstones contain abundant silt-sized grains and ductile gains, giving them lower permeabilities (Marchand et al., 2015).

Paleocene Lower Wilcox sandstone sediment routing and deepwater depositional areas for the Gulf of Mexico were earlier reconstructed by Galloway (2008), Galloway et al. (2011), and McDonnell et al. (2008) (Fig. 14). New well control (Fig. 13) suggests the thickest units of sandstone deposition are now are in the central part of the study area, implying that sand sources from the Hardin Canyon funnel and the Holly Springs Delta (Fig. 14) either overlapped, or sands from the Holly Springs Delta system completely overwhelmed the study area. The small starved basin to the west of the Hardin Canyon fan is apparent in Figure 13, just not as far to the west and with a southern extension. Recently published, revised sandstone maps, using newer well control, confirm the observed merger of previously separated deepwater fan systems (Snedden et al., 2018) (Fig. 15).

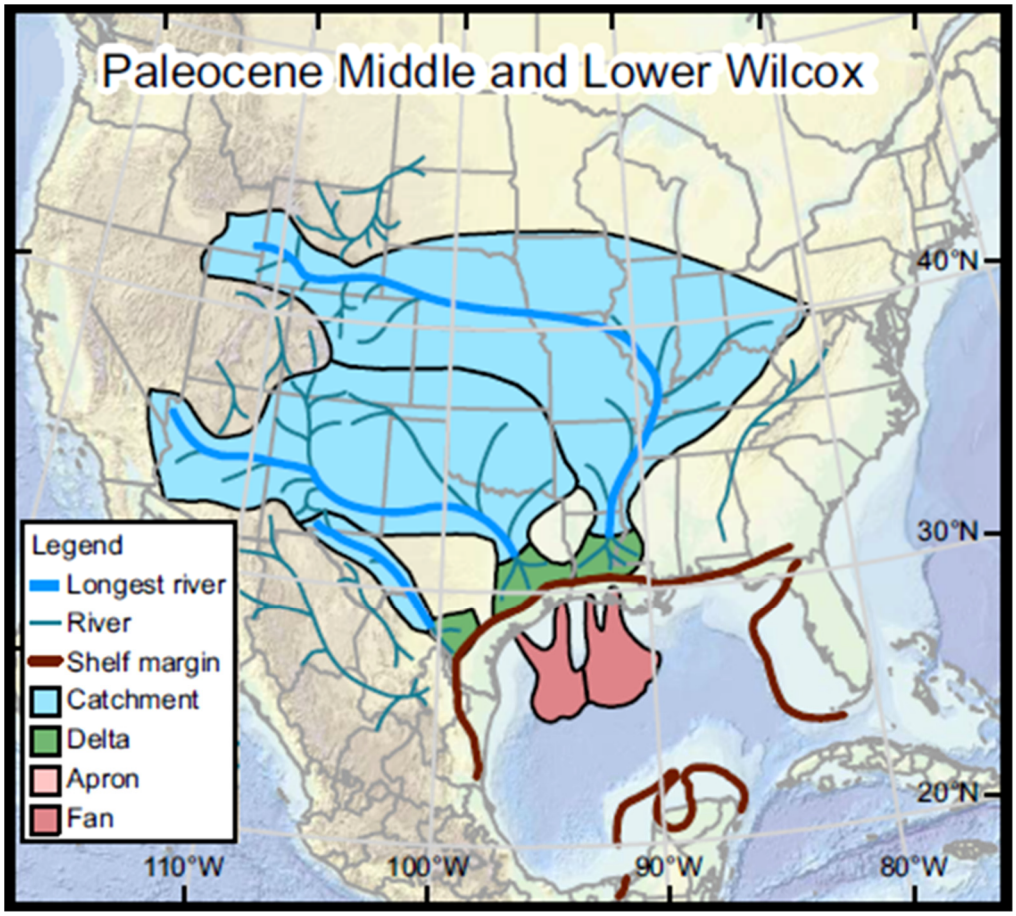

Figure 15. Recently updated sediment sourcing map for the Paleocene Middle and Lower Wilcox sandstones using current available well control. This agrees with Figure 13 (modified after Snedden et al., 2018).

Eocene Sandstone

Eocene sandstone thickness distribution is similar to that of the Paleocene except that the thickest sandstone units are shifted to the southeast in Walker Ridge with no hint of possible thicker units to the west (Fig. 16). However, three minor thickness trends are oriented from northwest to southeast: two in Keathley Canyon and one in Walker Ridge. The Upper Wilcox is the main contributor for sandstone deposition in this deepwater region; depositional trends probably reflect lobe shifting perpendicular to the paleo-transport trend (Galloway et al., 2000; Galloway, 2008). During the Eocene, the best Wilcox sands are in canyon fills and meandering channels (Cornish, 2013). The first deepwater well to encounter the Wilcox sandstone was drilled west of the study area in Alaminos Canyon block 600 in 1996 (Nixon et al., 2016). The highest volume fraction of Eocene sandstone is found in WR–372–001. The Upper Wilcox is early Eocene in age and the distribution of these sands in the Gulf of Mexico is shown in Figure 17.

Oligocene Sandstone

Sandstone deposition is much reduced in the Oligocene compared to other Cenozoic epochs (Fig. 18) with three zones of minimally "thick" sandstones: (1) southeast corner of Keathley Canyon; (2) northwest corner of Keathley Canyon; and (3) northeast section of Walker Ridge. In the Rio Grande Embayment of South Texas, the Oligocene Frio-Vicksburg interval has long been recognized as a prolific petroleum producer from shelf-edge delta sandstone reservoirs, but the thickest sandstones are confined to the Vicksburg detachment zone (Coleman and Galloway, 1990). Due to this structural accommodation and a generally arid climate, large volumes of sandstone did not reach the study area (Fig. 19). Similarly, the Texas and Louisiana Frio Formation, younger in age than the Vicksburg, is a prolific producer onshore and in shallow-water offshore wells (Hamlin, 1989; Swanson et al., 2013), but no Frio sands have been penetrated to date in the study area. However, Oligocene sandstones are present in deepwater confined channel systems at the Silvertip portion of the Great White Field area in the adjacent Alaminos Canyon protraction block (Eikrum et al., 2011).

Miocene Sandstone

There is a surprising similarity in the sandstone distribution for the Eocene, Miocene, and Pliocene. The thickest sandstone units are concentrated in the southeastern part of Walker Ridge, noting that this is at the limit of well data along the Sigsbee Escarpment. Both the Miocene and Pliocene sandstone isochore maps show a secondary thickness trend in central Keathley Canyon, indicative of possible slope fan presence. However, Miocene oil and gas production in the study area is more or less limited to the northern part of Walker Ridge and into the Green Canyon areas, implying that the Miocene sands in the main part of the study area lack hydrocarbon sourcing, or effective traps, or the porosity and permeability necessary for a good reservoir (Figs. 20). The highest volume fraction of Miocene sandstone is found in WR–249–001. Within the study area Miocene production is limited to the wells in Green Canyon, one field in

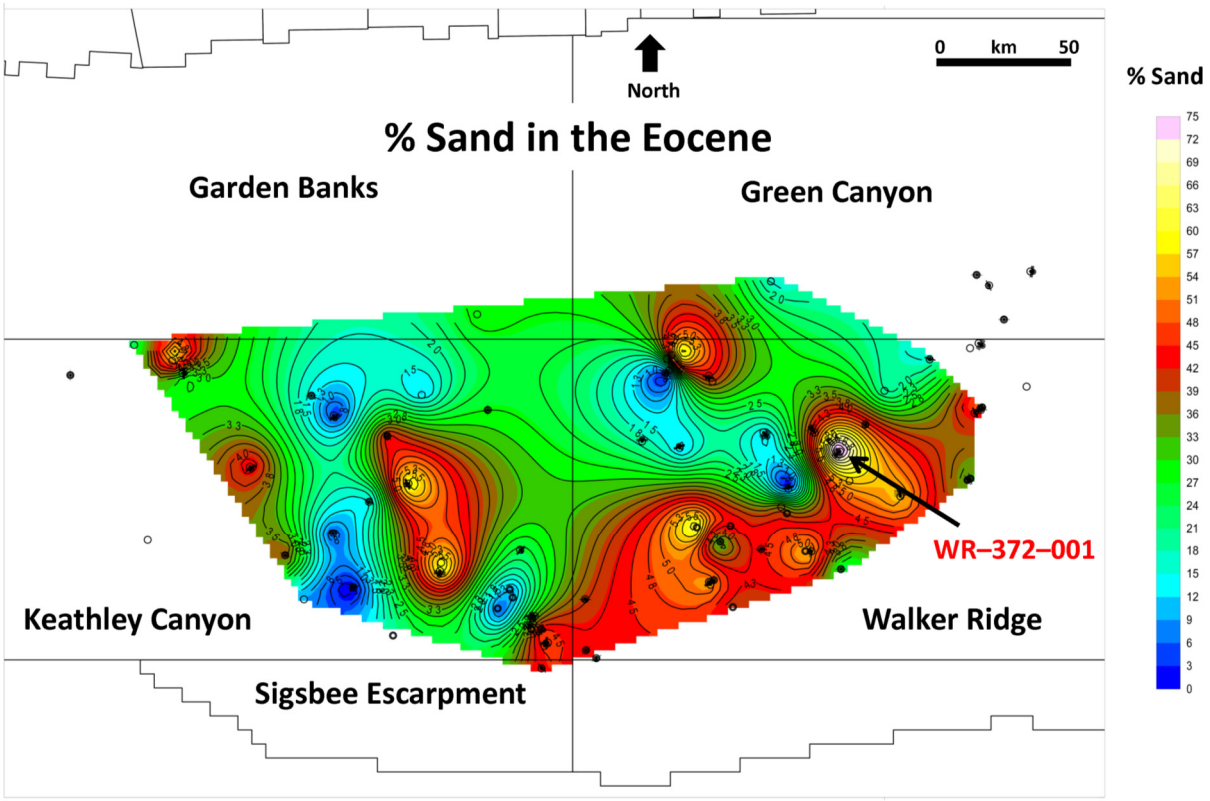

Figure 16. Map of percent (volume fraction) sandstone deposited during the Eocene Epoch. 50 km = ~31 mi.

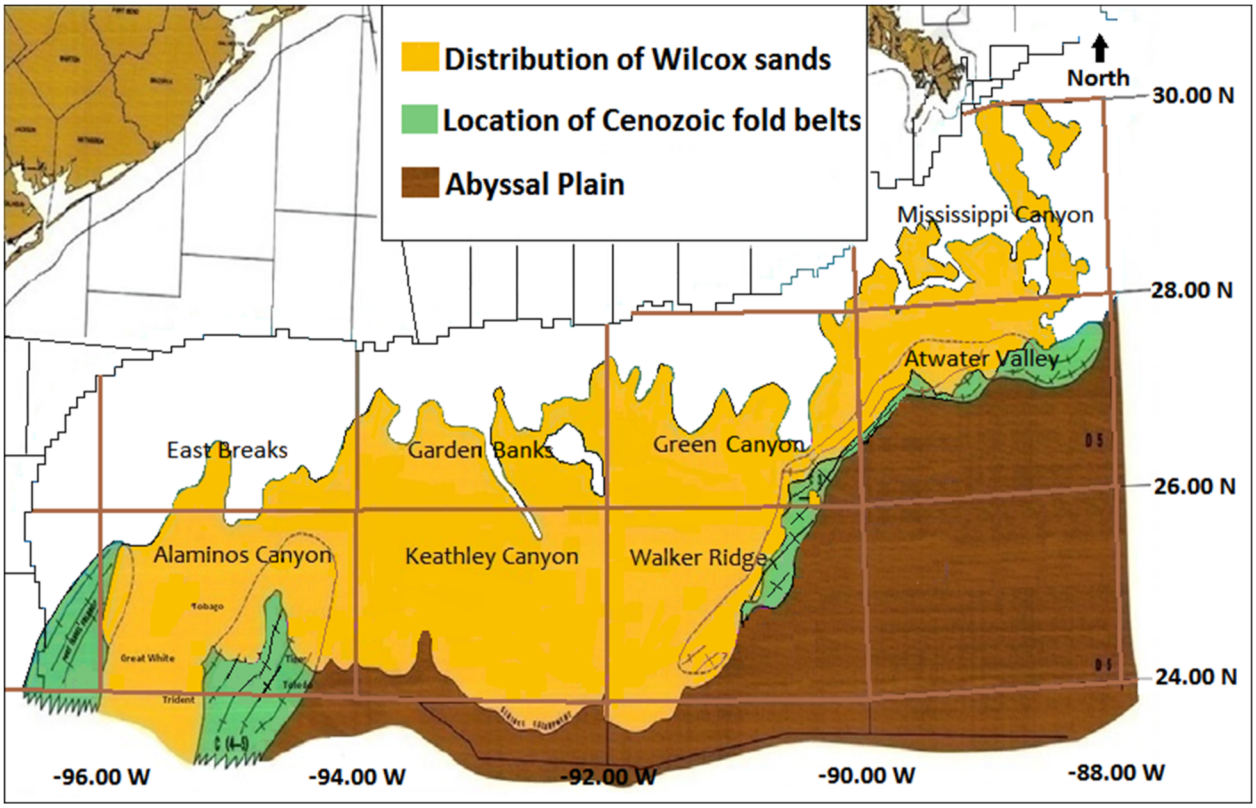

Figure 17. Distribution of the lower Eocene Upper Wilcox across the deepwater Gulf of Mexico Basin, shown in gold (modified after Rains et al., 2007). Fold belts are shown in green.

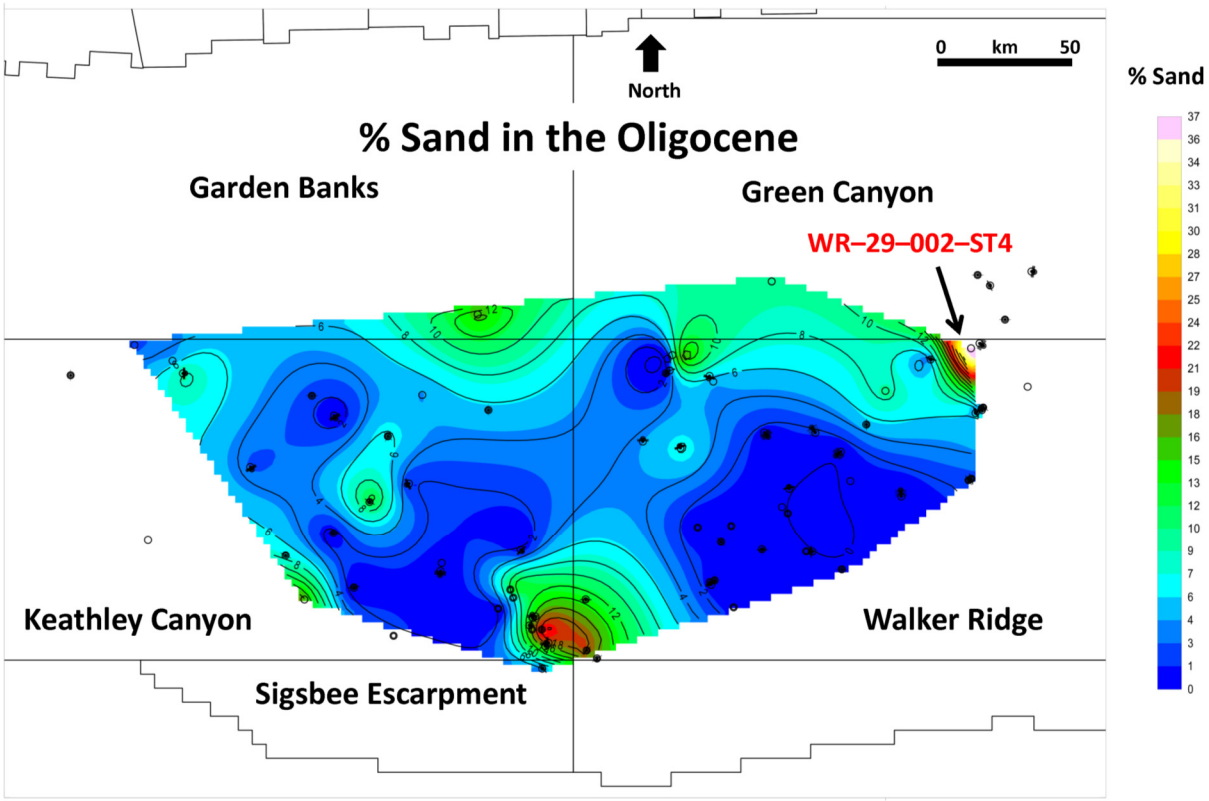

Figure 18. Map of percent (volume fraction) sandstone deposited during the Oligocene Epoch. 50 km = ~31 mi.

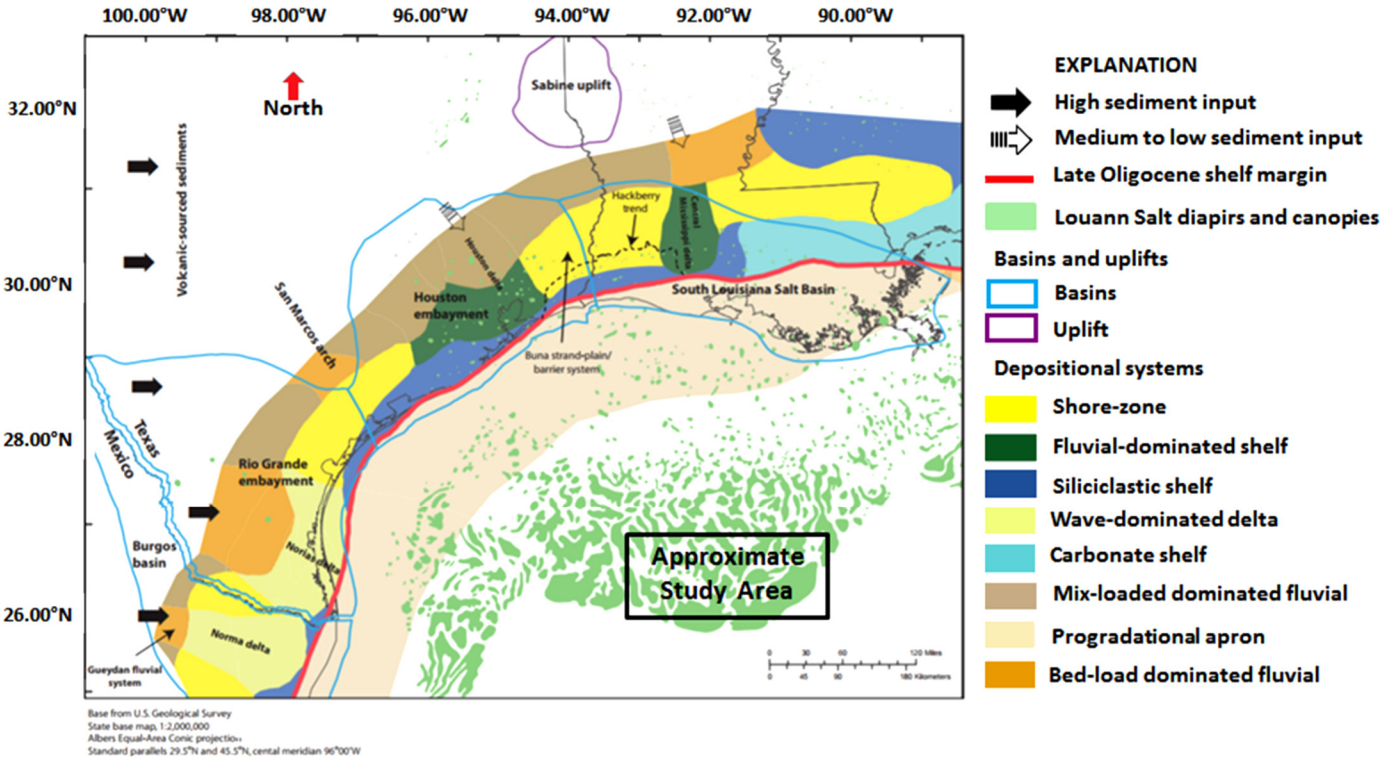

Figure 19. Oligocene Frio Formation progradational deposition largely landward of the coeval continental slope, thus large quantities of sandstone apparently never reached the deepwater study area of Keathley Canyon and Walker Ridge (modified after Swanson et al., 2013).

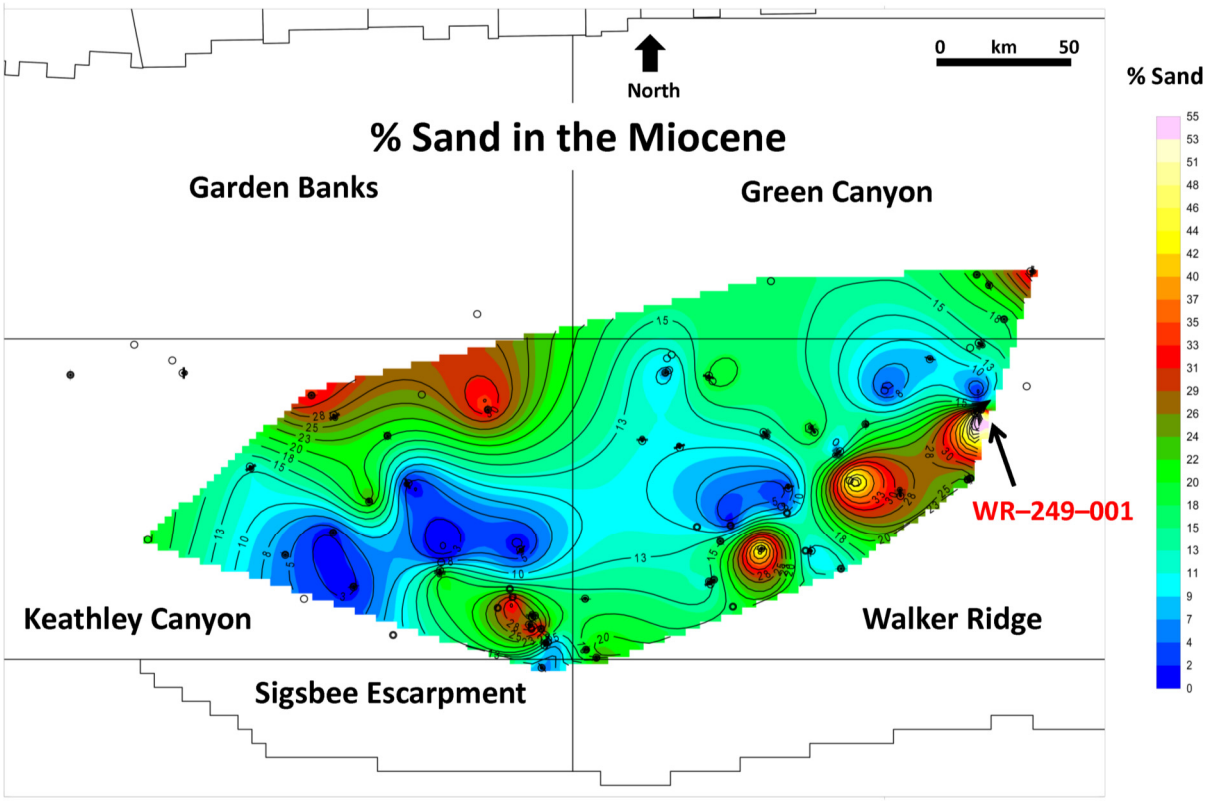

Figure 20. Map of percent (volume fraction) sandstone deposited during the Miocene Epoch. 50 km = ~31 mi.

northernmost Walker Ridge block 29, and a Miocene discovery in WR–160–001 drilled by Statoil in April 2015. According to Figure 21, which was produced from research done using seismic data at the Institute for Geophysics at the University of Texas in Austin, the thick Miocene sand deposition in central Walker Ridge (Fig. 20) must be middle to late Miocene in age.

Pliocene Sandstone

The thicker Pliocene sandstone intervals are located mainly inboard of the Sigsbee Escarpment in central Walker Ridge, wrapping around into southeastern Keathley Canyon (Fig. 22). However, there is a lack of Pliocene sandstone in eastern-central Keathley Canyon. There are four third-order lowstand systems tracts in the Pliocene (Miller et al., 2005), which could have caused periods of enhanced basinward transport into the Gulf of Mexico Basin from the central Texas coast all the way to Mobile Bay. However, sediment supply variations are equally important. There are two major sandstone depocenters developed in Keathley Canyon and two are also present in Walker Ridge. The Lucius and Hadrian South fields, in the southeastern corner of Keathley Canyon, produce from Pliocene-aged reservoirs. Only one of these wells drilled deep enough to penetrate the Paleocene Wilcox sands, but the well was plugged and abandoned (KC–919–001).

Note how the area of limited sandstone volume has a trend from northwest to southeast (Fig. 22), inside a more generalized zone of reduced-sandstone deposition that trends northeast to southwest, which is similar to the reduced-sandstone thickness trend in the Miocene (Fig. 20). The highest volume fraction of Pliocene sandstones is found in WR–460–001. During the Pliocene, the Mississippi River expanded its drainage area and began construction of the largest submarine fan in the Gulf of Mexico Basin (Weimer, 1989; Galloway, 2008). Pliocene fans formed east of Keathley Canyon (Fig. 23).

Pleistocene Sandstone

The Pleistocene sandstone distribution (Fig. 24) is dissimilar to that in the Pliocene (Fig. 22) except for similar trends in four localized areas: the areas around WR–848–001, KC–963–001–ST1 and KC–964–001, KC–627–001, and KC–255–001. Note that the area of no sandstone (colored pink) trends north to south instead of northwest to southeast as in the Pliocene Epoch. At the end of 2006, Pleistocene reservoirs in the Gulf of Mexico had produced 8.26% of the oil and 16.14% of the natural gas, Pliocene reservoirs had produced 40.59% of the oil and 31.57% of the natural gas, Miocene reservoirs had produced 50.95 % of the oil and 51.20% of the natural gas, while all other reservoirs dated pre-Miocene had produced only 0.20% of the oil and only 1.09% of the natural gas (Crawford et al., 2009; BSSE, 2018a). This was before the Wilcox exploration discoveries in 2007–2010. Pleistocene progradation and slope fans are more spread across the northern central Gulf of Mexico (Fig. 25) than the equivalent Pliocene deposits (Fig. 23). Pleistocene sandstone reservoirs have been prolific all across the shallow waters of the western and central Gulf of Mexico, numerous on the continental shelf, and even a few on the continental slope (BOEM, 2017).

Cenozoic Shale Distribution in the Study Area

The next most important depositional unit for the study area and the Gulf of Mexico in general, is shale. Shale is an important hydrocarbon source below the sandstone and frequently acts as a reservoir seal on top of the sandstone. The relationship between sandstone and shale is somewhat related in the Gulf of Mexico, for instance, along siliciclastic shorelines and shelves, where a large volume fraction of sand was deposited, there was a small volume fraction of mud, and vice versa. However, in deepwater systems, turbidites often deposit as much sand as fine-grained sediment as high-density flows grade into dilute flows. This

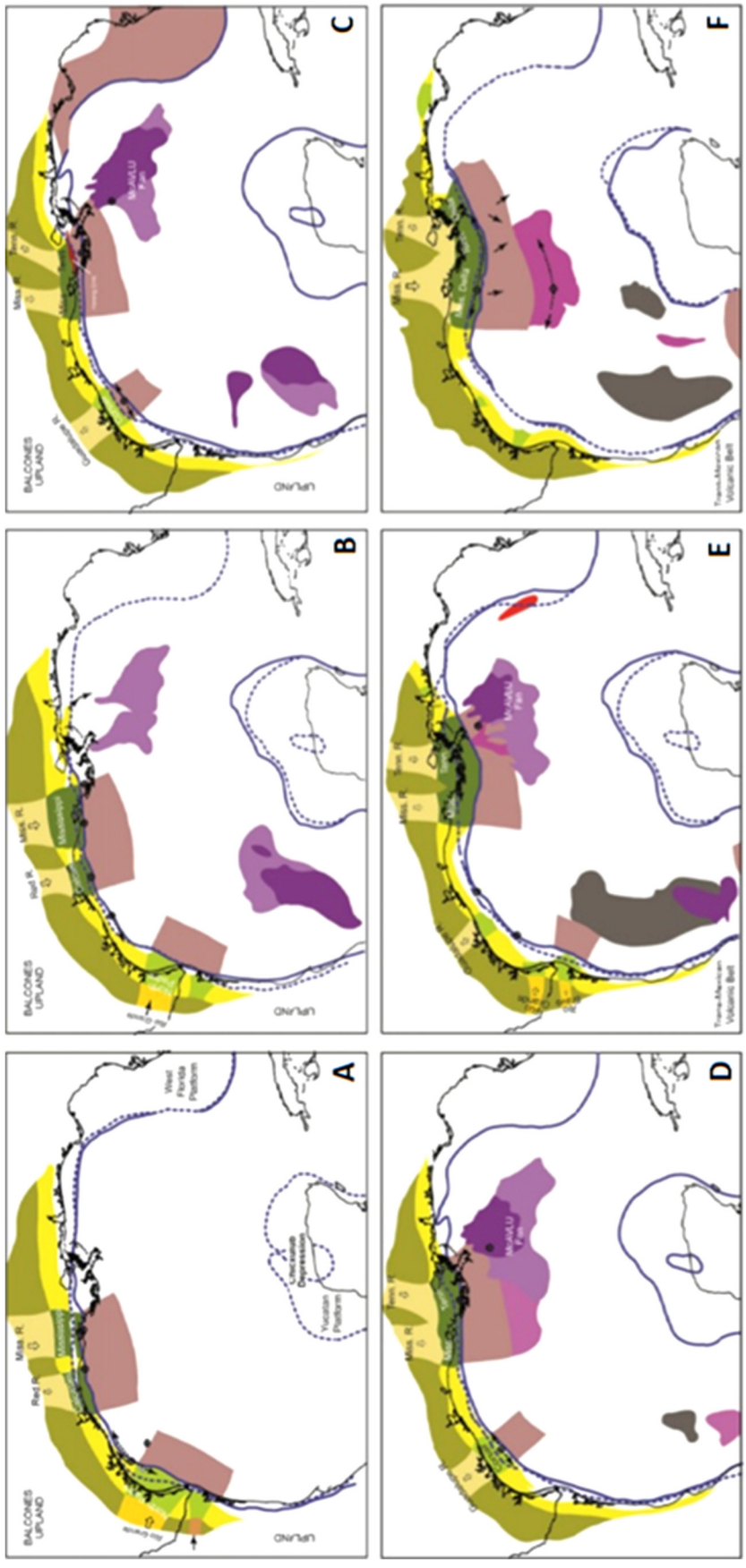

Figure 21. Miocene paleogeography for the Gulf of Mexico Basin (modified after Snedden et al., 2012). Note how the shift of deposition from the western to the eastern Gulf of Mexico is very prominent throughout the Miocene. The study area is inside the black box.

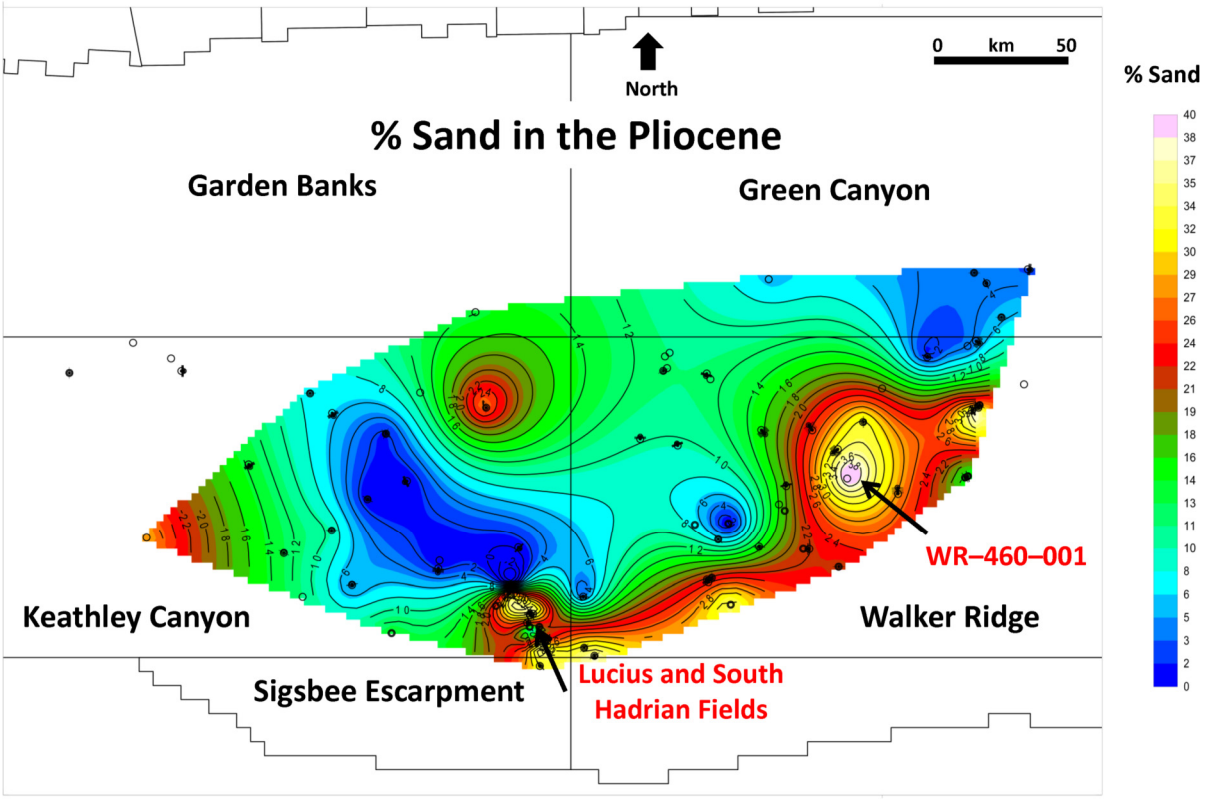

Figure 22. Map of percent (volume fraction) sandstone deposited during the Pliocene Epoch. 50 km = ~31 mi.

general inverse relationship is broadly true for the six Cenozoic epochs: Figure 26 (Paleocene), Figure 27 (Eocene), Figure 28 (Oligocene; Figure 29 shows Oligocene limestone and marl percentages), Figure 30 (Miocene), Figure 31 (Pliocene), and Figure 32 (Pleistocene).

The average shale volume fraction for each epoch is: Paleocene 46.19%, Eocene 46.37%, Oligocene 59.08%, Miocene 65.60%, Pliocene 66.29%, and Pleistocene 77.38%. These numbers tell us that the volume fraction of shale has been increasing over Cenozoic geologic time since the Paleocene and this trend is in sync with the decreasing amounts of sandstone being deposited in the same area over the same time span. The Neogene glaciation contributed to the diminished amount of suspended load in rivers draining into the Gulf of Mexico Basin (Galloway et al., 2011).

Shales deposited in deepwater settings display characteristic features that reflect distinct depositional and post-depositional processes, which may be used to predict reliable depositional facies distributions observed on seismic data (Almon et al., 2009). Analyses of Cenozoic-aged shales from deepwater depositional settings in offshore West Africa, offshore Brazil, and the Gulf of Mexico reveal the common occurrence of six shale microfacies. Each shale microfacies exhibits distinct textures and fabrics that represent variations in depositional environment. A systematic pattern of seal capability is evident when these shale types are organized within a sequence stratigraphic framework. In general, silt-poor shales (representing upper transgressive units) and some condensed shale units offer seal potentials from good to excellent. In comparison, silt-rich highstand shales and silt-rich lowstand shales have relatively low-sealing capacity, demonstrated by mercury injection capillary pressure measurements. Increasing the volume fraction of silt grains reduces the sealing capacity by inhibiting mechanical compaction. Seal quality generally increases as total clay and carbonate content increases (Almon and Dawson, 2004). In the last section, where we look at the siltstone contour maps, they will be paired with the shale maps to look for areas of overlap. However, seal capacity is also a function of post-depositional processes such as mechanical failure, a common occurrence around Gulf of Mexico salt structures where large hydrocarbon columns can destroy the top seal (Dawson and Almon, 2002).

Paleocene Shale

The aforementioned inverse relationship between sandstone and shale content is demonstrated by comparing the two Paleocene maps (Figs. 13 and 26). For the Paleocene Epoch, there was a large area of sandstone deposition; but in those areas that did not receive much sand, there is a large percentage of shale.

Eocene Shale

The inverse relationship between volume fractions of Eocene shale and sandstone is also apparent (Figs. 16 and 27). The thickest shale deposits are to the west, as compared to the Paleocene shale deposits. It is important to point out that the maps depict only a gross distribution of sandstone and shale volume fractions during the Eocene because most of the sandstone was deposited in the Lower Eocene (Upper Wilcox depisode as defined by Galloway [2008]) and most of the shale was deposited during the Middle and Upper Eocene (Sparta, Queen City, and Yegua depisodes); i.e., the highest volume fractions of both lithologies were not contemporaneous.

Oligocene Shale

In the Oligocene, climatic conditions and reduced accommodation space (caused by tectonics inland of the study area) limited the transport of sand-sized grain material (Snedden et al.,

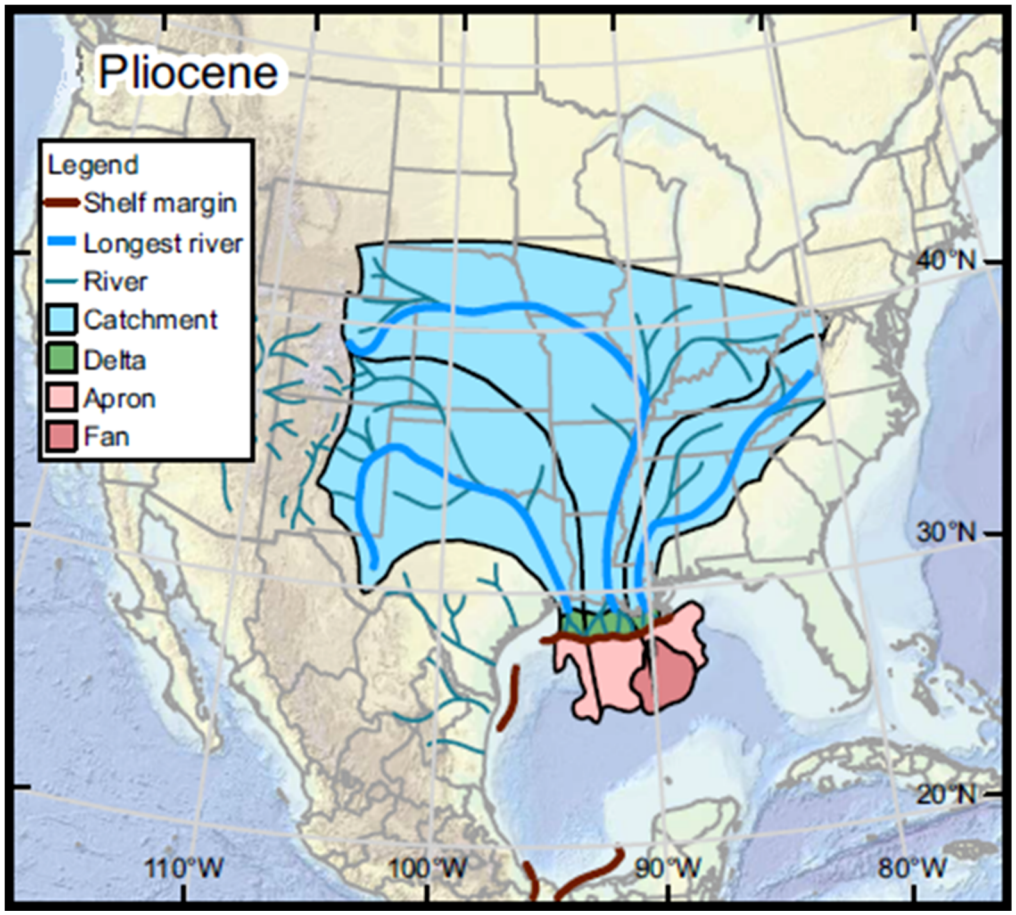

Figure 23. Limits of Pliocene sandstone deposition into the Gulf of Mexico Basin (modified after Snedden et al., 2018). Note the eastward drift of sediment sourcing moving away from the Texas coastline to that of Louisiana and Mississippi.

2012). Dissolved $CaCO_3$ in the water precipitated to the seafloor to form micritic limestone or marl, depending on the amount of silt or clay already on the seafloor (Folk, 1959). This will be discussed in more detail in Part 2 (Cornelius and Emmet, 2018b, this volume). The inverse relationship between sandstone and shale still exists, but it has been masked somewhat due to the noticeable presence of the limestone, marl, and siltstone components (Figs. 18, 29, and 35).

Miocene Shale

The inverse relationship between sandstone and shale deposition is much more apparent in the Miocene (Figs. 20 and 30). The far greater volume fractions of shale during the Miocene and the presence of only three wells with Miocene production in the study area suggest that most sediment reaching the study area was fine to very fine grained. Sea-level fall, beginning in the mid-Oligocene, continued into the Miocene, and along with cooler temperatures affected sedimentation coming into the deep basin (Miller, 2009).

Pliocene Shale

Shorter transgressive-regressive cycles dominate the Pliocene with 30% less sandstone reaching the study area than sandstone of Miocene age. Sediment starvation within a large portion of Keathley Canyon resulted in deposition of very significant volumes of shale (Fig. 31).

Pleistocene Shale

Pleistocene transgressive-regressive cycles are similar in number and intensity to those occurring in the Pliocene. There was significant influence from Pleistocene glaciation with its effect on erosion and pulses of meltwater to the basin (Galloway et al., 2011). However, the sandstone volume fraction is down 25% from that in the Pliocene and consequently the geographic areas with large volume fractions of shale deposition have noticeably increased (Fig. 32).

Cenozoic Siltstone Distribution in the Study Area

Siltstone accumulates in sedimentary basins throughout the world and the Gulf of Mexico is no exception. Its presence represents a level of energy, which brought silt to its current location before lithification, intermediate between that required to move larger sandstone grains and the finer-grained mud. For most basins, siltstone is less common than either sandstone or shale, and this is also true for the Gulf of Mexico. Siltstone rock units are usually thinner in accumulated thickness and less extensive laterally than either sandstone or shale. Examination of many deepwater cores has revealed that many of the alleged shales have a large silt component and are closer to siltstones rather than shales (Scott and Bouma, 2004). The siltstone volume fractions (%) per geologic epoch are displayed in Figure 33 (Paleocene), Figure 34 (Eocene), Figure 35 (Oligocene), Figure 36 (Miocene), Figure 37 (Pliocene), and Figure 38 (Pleistocene).

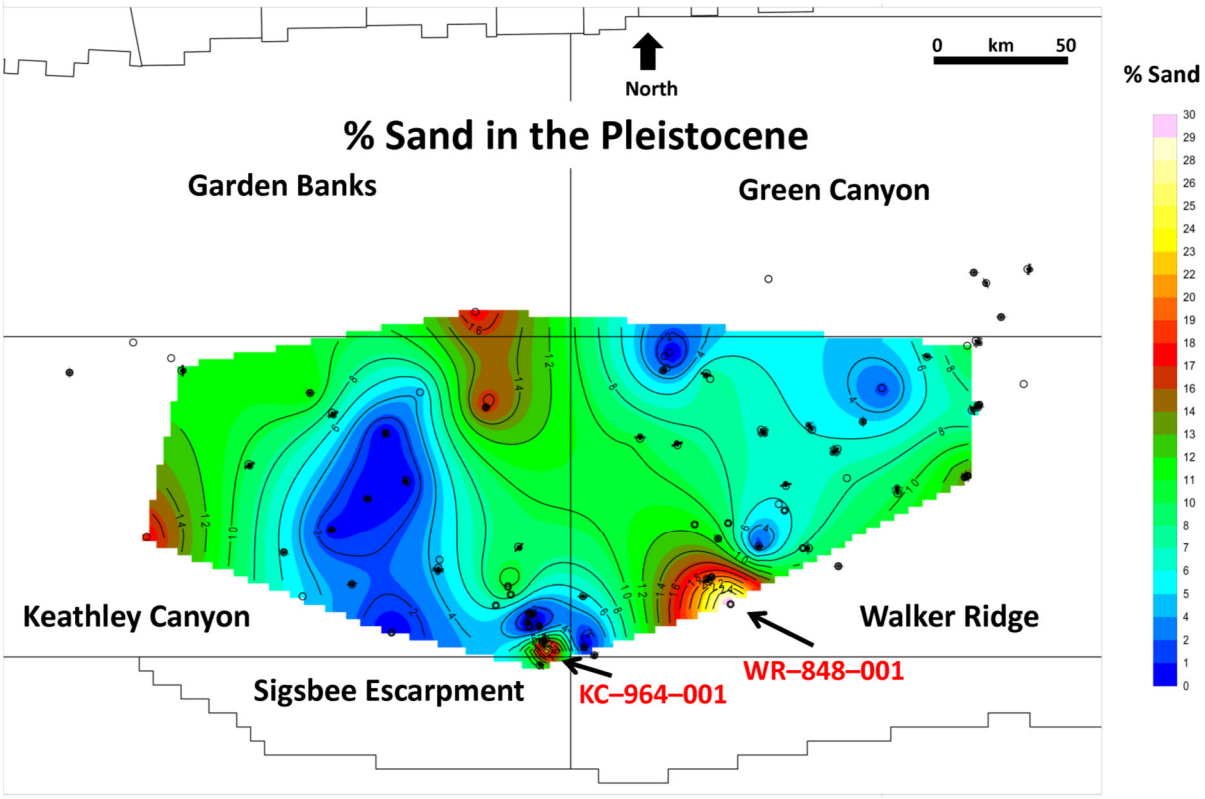

Figure 24. Map of percent (volume fraction) sandstone deposited during the Pleistocene Epoch. 50 km = ~31 mi.

Because shale that is deposited in the presence of siltstone results in an imperfect seal for hydrocarbons (Almon and Dawson, 2004), the isochore maps for the volume fractions of siltstone have been compared with those of shale for the same epochs to see if any insights can be gained. Our volume fraction calculations for any given epoch do not differentiate between siltstone that was deposited alone, without a shale component, and siltstone that was deposited with a significant shale component, and thus the sealing capability of the shale cannot be rigorously evaluated from our data.

Paleocene Siltstone

Even though turbidity flows transport both sand and silt to the deepwater environments, there was a much larger volume of Paleocene sandstone deposited within the study area. The area of a siltstone void (deeper blue zone) in Walker Ridge is also an area with high volume fractions of shale, and interestingly contains Wilcox production in Julia Field, Jack Field, and St. Malo Field, suggesting that the shale (in absence of siltstone) was able to form adequate seals over the reservoirs. The highest Paleocene siltstone volume fraction is found in KC–596–001, where it is 40.82% and the sandstone content is only 13.88%; thus there is no Wilcox reservoir (Fig. 33). However, there are many more factors to consider in determining a reservoir's viability; this aspect is only one of them.

Eocene Siltstone

The highest concentration of Eocene siltstone is centered on the KC–414–001 well where the siltstone volume fraction is 41%, the Eocene shale volume fraction is only 14%, but the Eocene sandstone volume fraction is 44.5%. However, the end-of-well report (EOWR) for this well (obtained from BSEE) shows that the shale above the Wilcox 1 sand is both silty and very calcareous, meaning that it is not an effective reservoir seal. Deeper in the borehole (the Lower Eocene) the calcareous elements in the shale disappear but the silty elements in the shale remain. This well was not a Wilcox discovery in spite of the thick sandstone reservoir units present (Fig. 16).

Oligocene Siltstone

The same climatic conditions and overall sediment sequestration in the Vicksburg detachment zone onshore that limited the routing of sand-sized grains to the study area, also limited the amount of siltstone. The small amounts of sandstone and siltstone that were deposited are located on the northern fringes of the study area (Figs. 18 and 35). The areas that are void or nearly void of siltstone are blanketed by high volume fractions of shale (Fig. 28), thus exhibiting an inverse relationship. The GB–959–001–BP1 well at the northern edge has the highest volume fraction of Oligocene siltstone.

Miocene Siltstone

Very small amounts of siltstone were deposited during the Miocene because of the much larger volume fractions of sand deposited. Apparently, the transport mechanism was sufficiently robust to carry the larger grain sizes to the study area, diluting the volume fraction of siltstone. Note the depositional axis for the siltstone is the same northeast-southwest trend as the sandstone deposits (Figs. 36 and 20), which is what is expected considering the middle and upper Miocene depocenters are to the northeast of the study area (Fig. 21). Again, there is an inverse relationship between the amounts of siltstone and shale in this region. The largest Miocene siltstone volume fraction was in the WR–282–001 well.

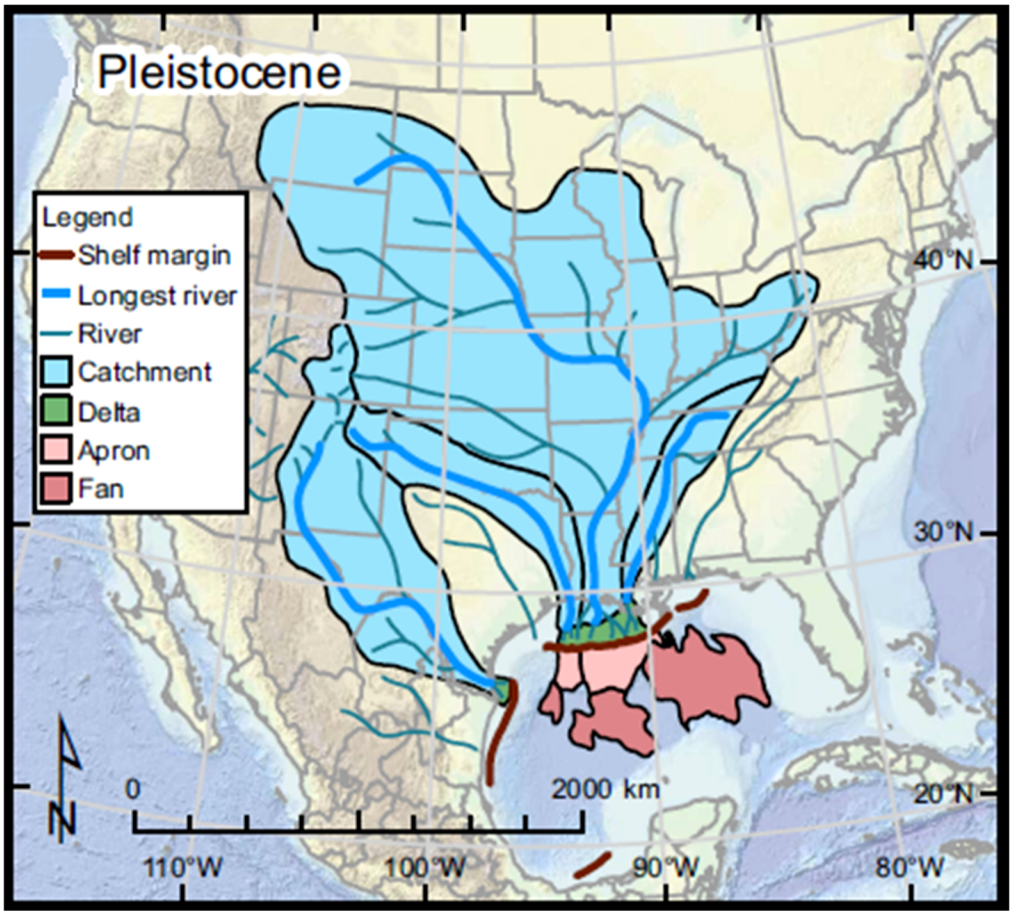

Figure 25. Limits of Pleistocene sandstone deposition in the Gulf of Mexico Basin from various drainage bases across the U.S. (modified after Snedden et al., 2018). Note the continuing shift of deposition eastward.

Pliocene Siltstone

The absence of siltstone in western portions of the map, together with high percentages of shale, previously observed in the Oligocene, is a pattern in that is repeated in the Pliocene but shifts to the southeast and still within the Keathley Canyon study area (Fig. 37). Interestingly, to the immediate south, there is Pliocene production from sands in the Lucius and Hadrian South Fields. Note the Pliocene depositional axis also trends northeast to southwest, as expected (Fig. 8).

Pleistocene Siltstone

There is significant difference in the Pleistocene volume fractions in that sandstone and siltstone show a parallel relationship (Figs. 38 and 24) instead of an inverse one; the tendency is for both to occur together or not at all. However, both siltstone and sandstone maintain an inverse relationship with shale. This parallel relationship could possibly be caused by failure along the shelf edge, which might have generated debris flows (mass transport) of sediment with a higher percentage of siltstone to be deposited farther into the basin.

DISCUSSION

These sub-regional maps that depict Cenozoic deposition give an overview of temporal trends and lateral lithologic variations in a small portion of a large sedimentary basin. Most of these depositional trends were expected in light of previous basin-scale work; but some were not, reflecting local lobe shifting within several large abyssal fan systems. The expected trends are those that show the depositional axis to be more or less in alignment with the sediment source direction, such as the Eocene, Miocene, and Pliocene isochore maps. The unexpected trends are those that show the depositional axis to be either perpendicular to the sediment source direction, or for the depositional unit to be in an odd place relative to the direction of the sediment source, such as the Wilcox sands for the Paleocene and Eocene, as well as the Pleistocene isochore map. Of course, many accidents of transport may be experienced by sediment on its way to a final depositional location: debris flows, faulting, depositional lobe switching, or salt movement. For example, the Pleistocene and Pliocene depositional trends, in their respective epoch isochores, are perpendicular to one another. Possibly, it is because so much of the original Pleistocene and Pliocene deposition has been displaced by salt; and we are only observing a partial view of the original Plio-Pleistocene depositional trends.

Sandstone and siltstone do show an inverse relationship (when one component has a high percentage and the other has a low percentage) during both the Paleocene and the Eocene. There is less sandstone and siltstone within the study area during the Oligocene, because of generally arid conditions restricting river discharge and updip tectonic accommodation (Galloway et al., 2011), so no definitive comparison can be made. The shift in this inverse relationship began in the Miocene, where the inverse relationship maintained in the Walker Ridge protraction block, but a parallel relationship (both components are roughly the same percentage) is apparent in Keathley Canyon. These two different relationships also occur during the Pliocene, but they are distributed differently in the sense that there is a similar reduction of siltstone and sandstone in the central region of the study area; but

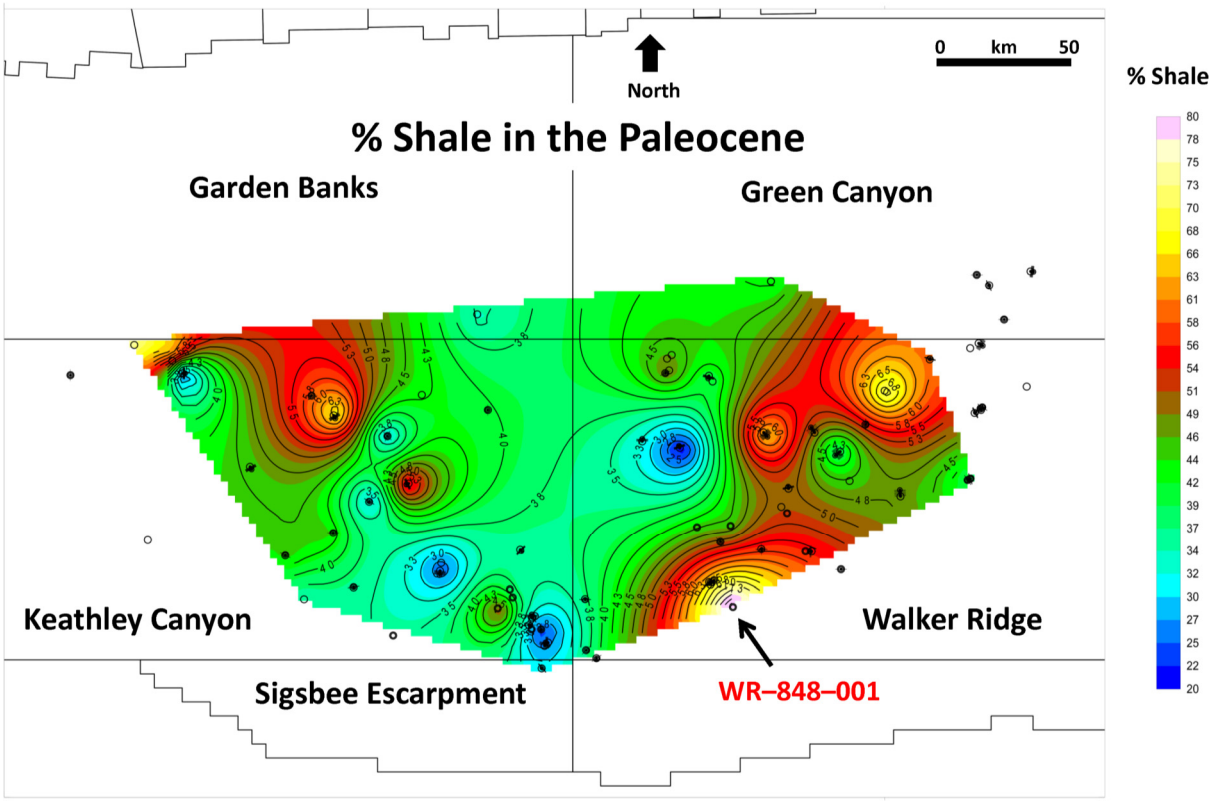

Figure 26. Map of percent (volume fraction) shale deposited during the Paleocene Epoch. For comparison to Paleocene sandstone percentage, please see Figure 13. 50 km = ~31 mi.

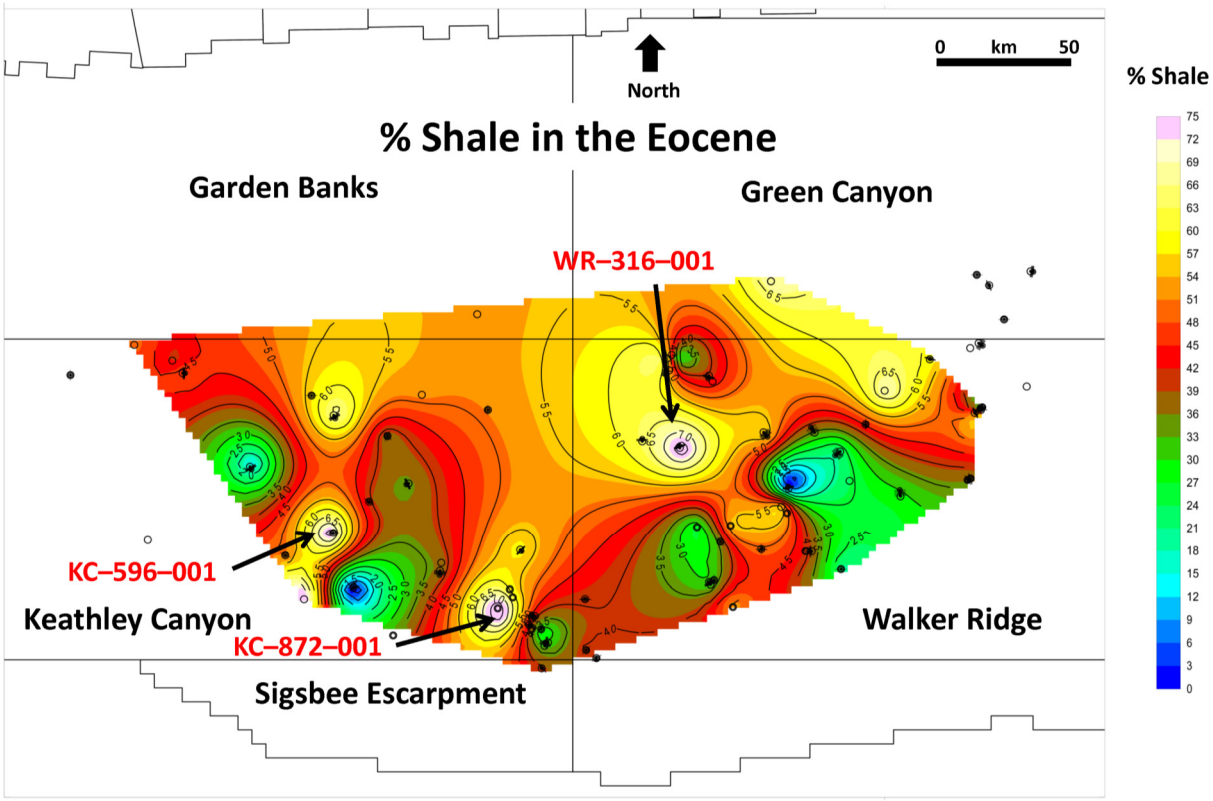

Figure 27. Map of percent (volume fraction) shale deposited during the Eocene Epoch. For comparison to Eocene sandstone percentage, please see Figure 16. 50 km = ~31 mi.

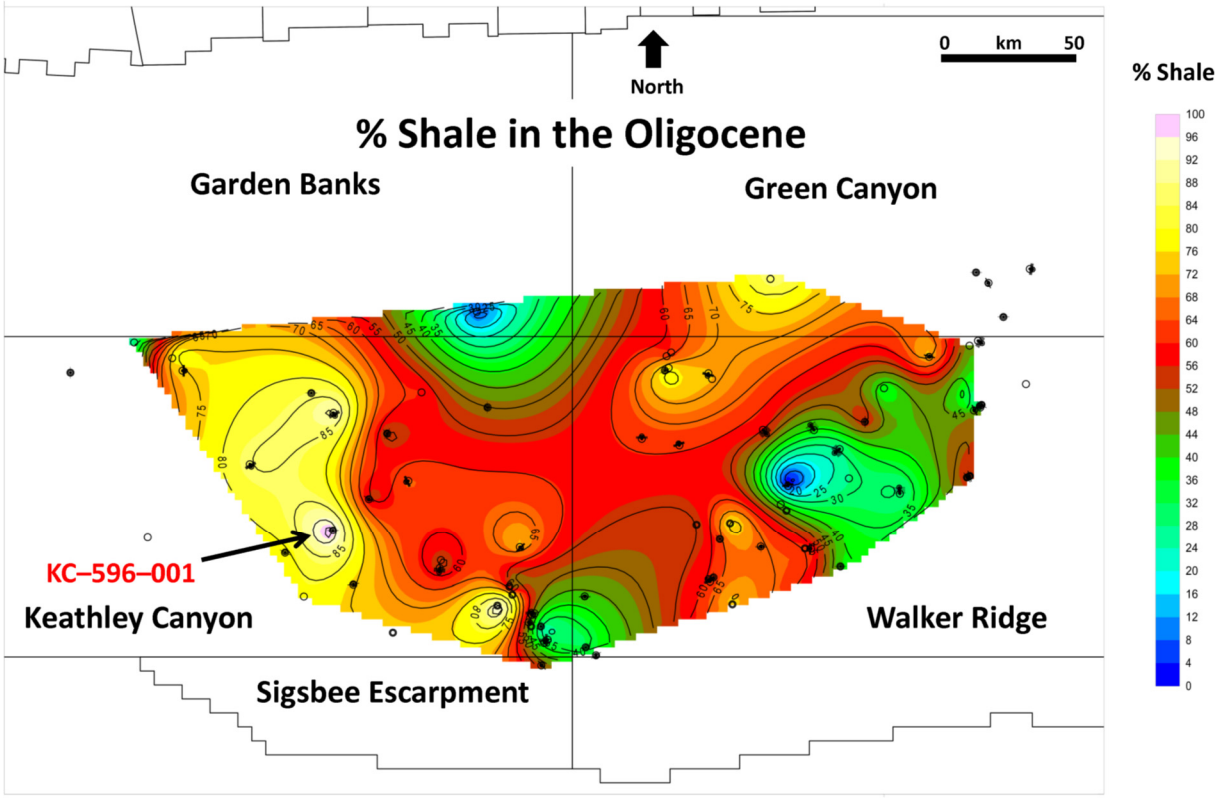

Figure 28. Map of percent (volume fraction) shale deposited during the Oligocene Epoch. The highest percentage of Oligocene shale was found in the KC-596-001 well. For comparison to Oligocene sandstone percentage, please see Figure 18. 50 km = ~31 mi.

the inverse relationship is consistent around the periphery. By Pleistocene time, the parallel relationship is consistent over the whole study area. The inference here is that there has been a significant change in the sediment source material.

CONCLUSIONS

There is so much new information presented on a regional basis in this study that it will take time to investigate the nuances of the comparative relationships and whether there are significant geological relationships contained therein. This study is only a preliminary look at the data with statements made on the readily obvious observations. Two of the more important observations are the inverse relationship between sand and shale deposition and the inverse relationship between sand and siltstone deposition. Both observations make geological sense; but are not necessarily intuitive over such a large regional area. It will take time and additional studies to delineate the more subtle comparisons because of the sheer volume of data.

We acknowledge a possible source of error in determining biostratigraphic age boundaries, which is not always precise since fossils usually have overlapping age ranges. Last appearance datums were used when they were available. Another possible source of error is in the identification of maximum flooding surfaces on well logs, which, given the large volumes of shale in the deepwater study area, is an interpretive exercise that adds some ambiguity to our results. The work presented here is in general agreement with earlier published literature from a variety of sources: academic, governmental, and industrial. Studies by authors affiliated with the University of Texas (e.g., Fulthorpe et al., 2014; Galloway et al., 2000, 2011; Galloway, 2008; Hamlin, 1989; Hudec and Jackson, 2011; Snedden et al., 2012; Zhang et al., 2017; etc.) with their regional compilations of sedimentation rate charts and Cenozoic depositional maps are in general agreement with data presented here. The reports from the U.S. Geological Survey (USGS) and BOEM (Swanson et al. [2013] and Nixon et al. [2016], respectively) are consistent with our maps of sediment thickness per geological epoch inasmuch as their data base did not include as many analyzed wells as were used in this study. Industry authors (e.g., Fiduk et al., 2014, 2016; Fiduk, 2017; Marchand et al., 2015; Rains et al., 2007; Rosenfeld, 2014) added details that enriched the data presentation in general. Most of the existing literature references were based on seismic data, a combination of seismic data with scattered well control, or in the case of the Marchand study, core samples. This study was based entirely on well logs, mud logs and paleontological data.

ACKNOWLEDGMENTS

We wish to thank Dr. Walter Wornardt of Micro-Strat, Inc. for checking some of the paleontological age determinations, Dr. Peter Vail is acknowledged for teaching both of us sequence stratigraphy when we were graduate students at Rice University, and IHS Markit for suggestions on how best to utilize their software application (Kingdom 2017). We also wish to thank our reviewers, Dr. Katie Joe McDonough and Dr. John W. Snedden, for their thoughtful comments and meaningful suggestions.

REFERENCES CITED

Almon, W. R., and W. C. Dawson, 2004, Seal character and variability within deep-marine depositional systems: Seal quantification and prediction: American Association of Petroleum Geologists Search and Discovery Article 40125, Tulsa, Oklahoma, 8 p., <http://www.searchanddiscovery.com/documents/2004/dawson02/> Last accessed August 21, 2018.

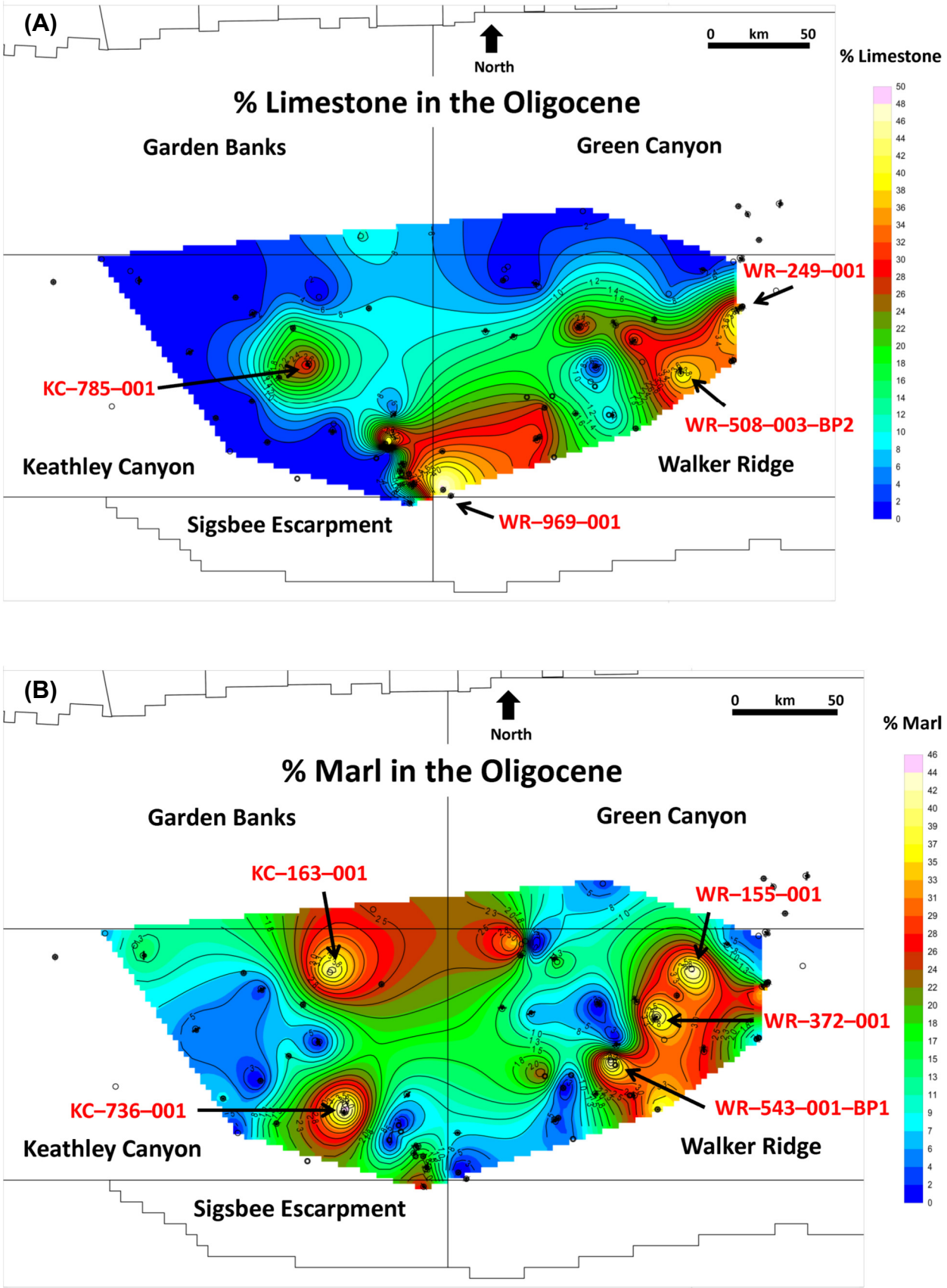

Figure 29. The higher volume fractions of both (A) limestone and (B) marl in the Oligocene (from Cornelius and Emmet, 2018b, this volume) somewhat masks the inverse relationship between Oligocene sandstone and shale. 50 km = ~31 mi.

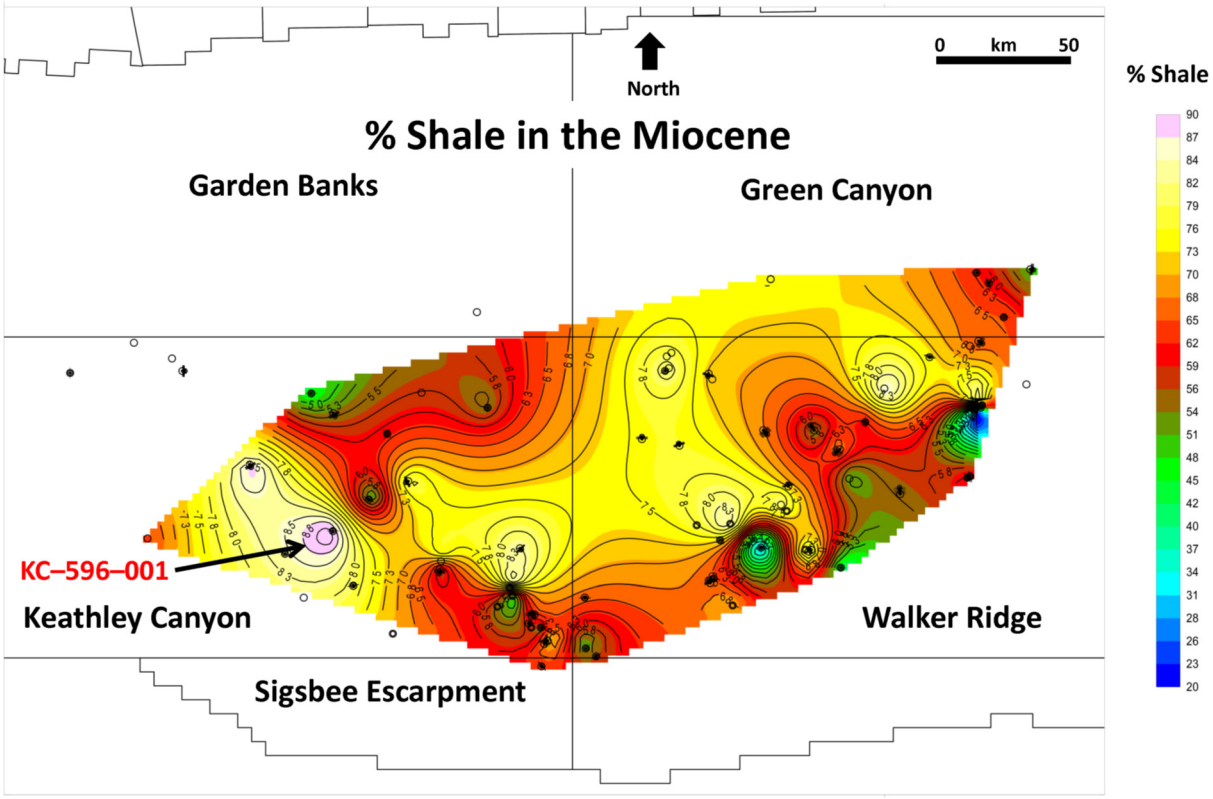

Figure 30. Map of percent (volume fraction) shale deposited during the Miocene Epoch. For comparison to Miocene sandstone percentage, please see Figure 20. The highest percentage of Miocene shale was found in the same KC–596–001 well that had the highest percentage of Oligocene shale (Fig. 28). 50 km = ~31 mi.

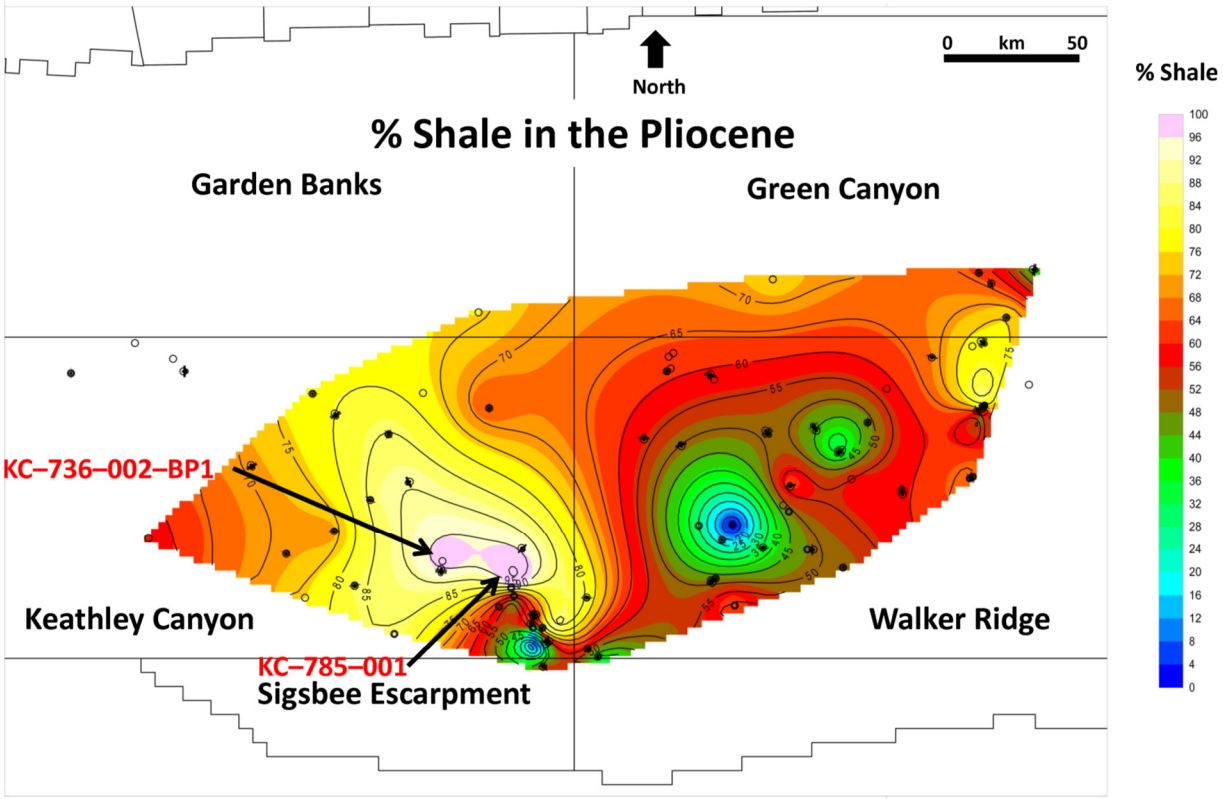

Figure 31. Map of percent (volume fraction) shale deposited during the Pliocene Epoch. For comparison to Pliocene sandstone percentage, please see Figure 22. 50 km = ~31 mi.

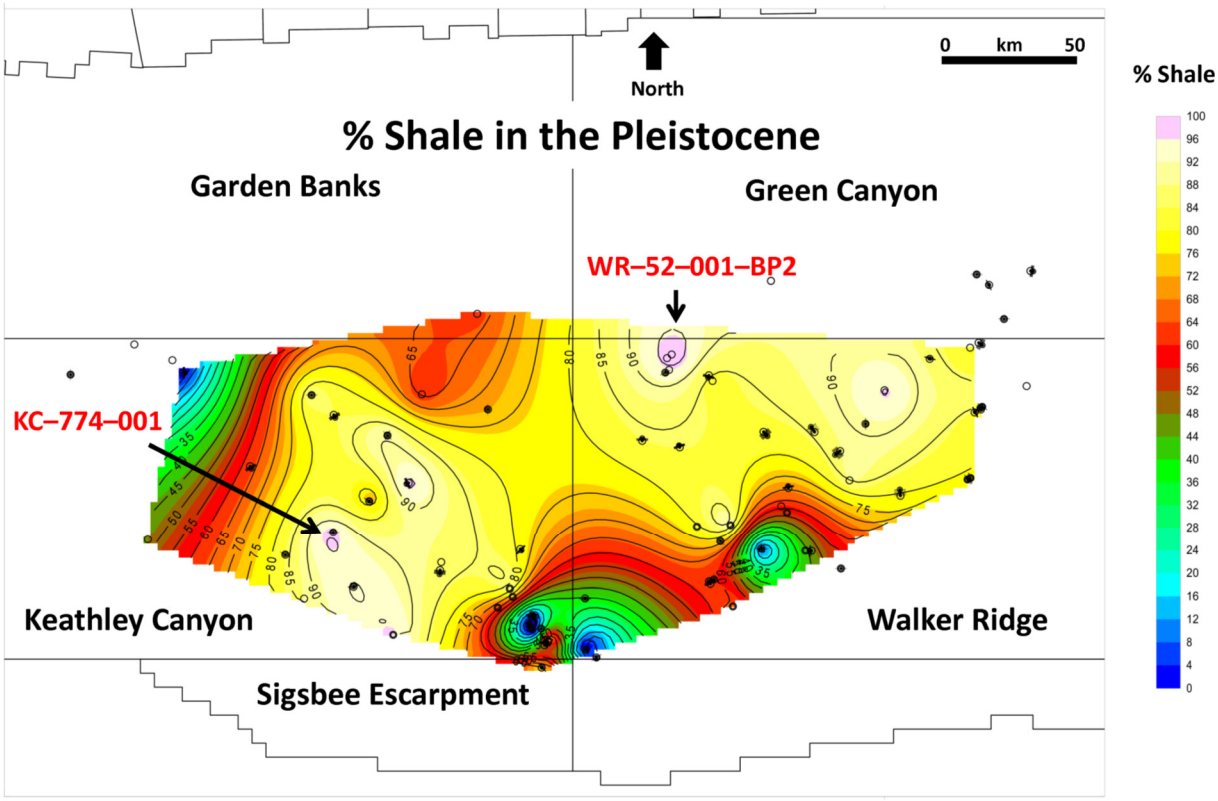

Figure 32. Map of percent (volume fraction) shale deposited during the Pleistocene Epoch. For comparison to Pleistocene sandstone percentage, please see Figure 24. 50 km = ~31 mi.

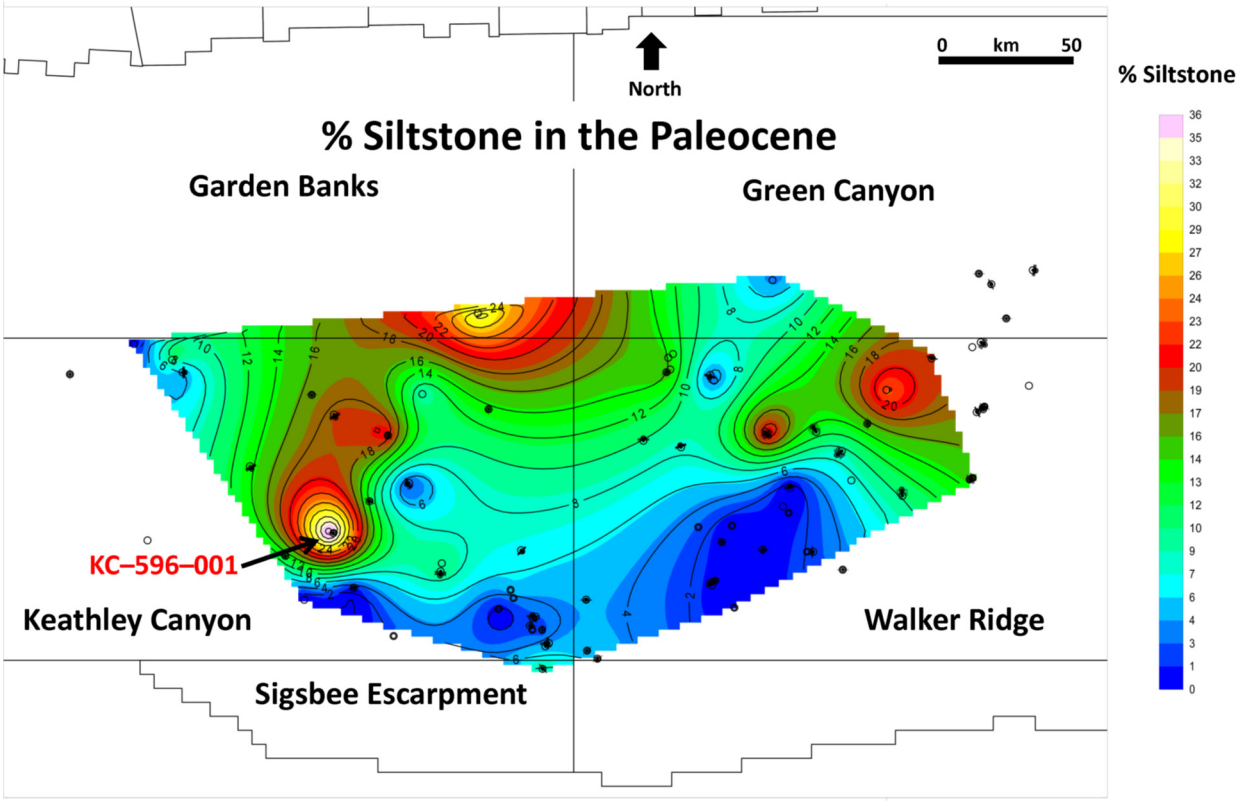

Figure 33. Map of percent (volume fraction) siltstone deposited during the Paleocene Epoch. For comparison to Paleocene shale percentage, please see Figure 26. 50 km = ~31 mi.

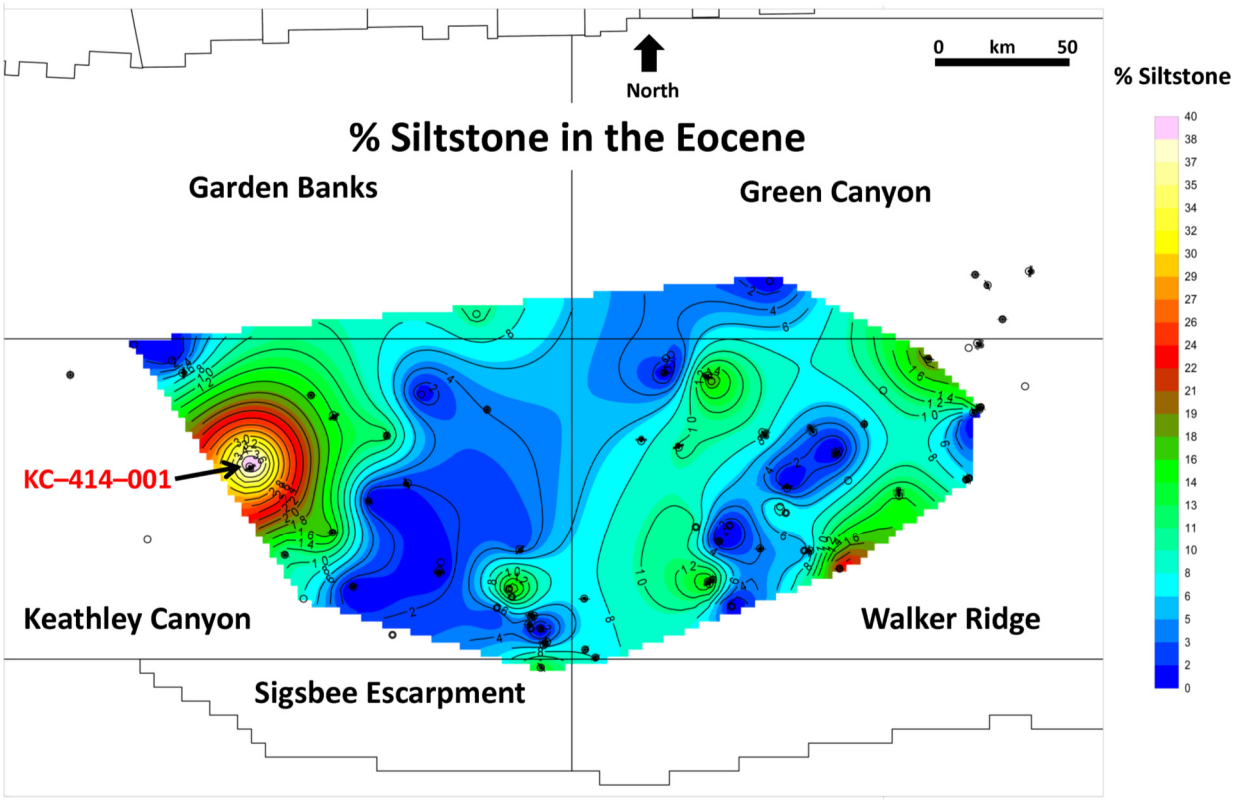

Figure 34. Map of percent (volume fraction) siltstone deposited during the Eocene Epoch. For comparison to Eocene shale percentage, please see Figure 27. 50 km = ~31 mi.

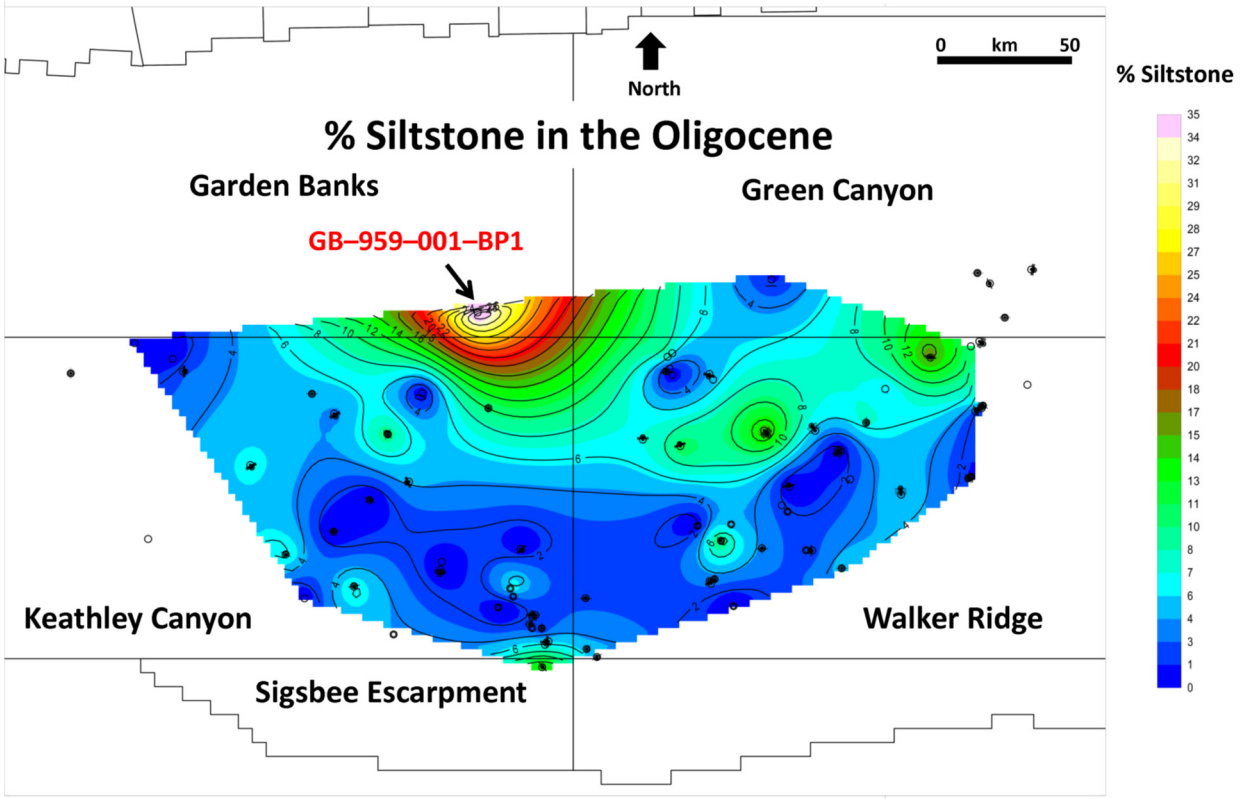

Figure 35. Map of percent (volume fraction) siltstone deposited during the Oligocene Epoch. For comparison to Oligocene shale percentage, please see Figure 28. For this epoch, there appears to be an inverse relationship between siltstone and shale. 50 km = ~31 mi.

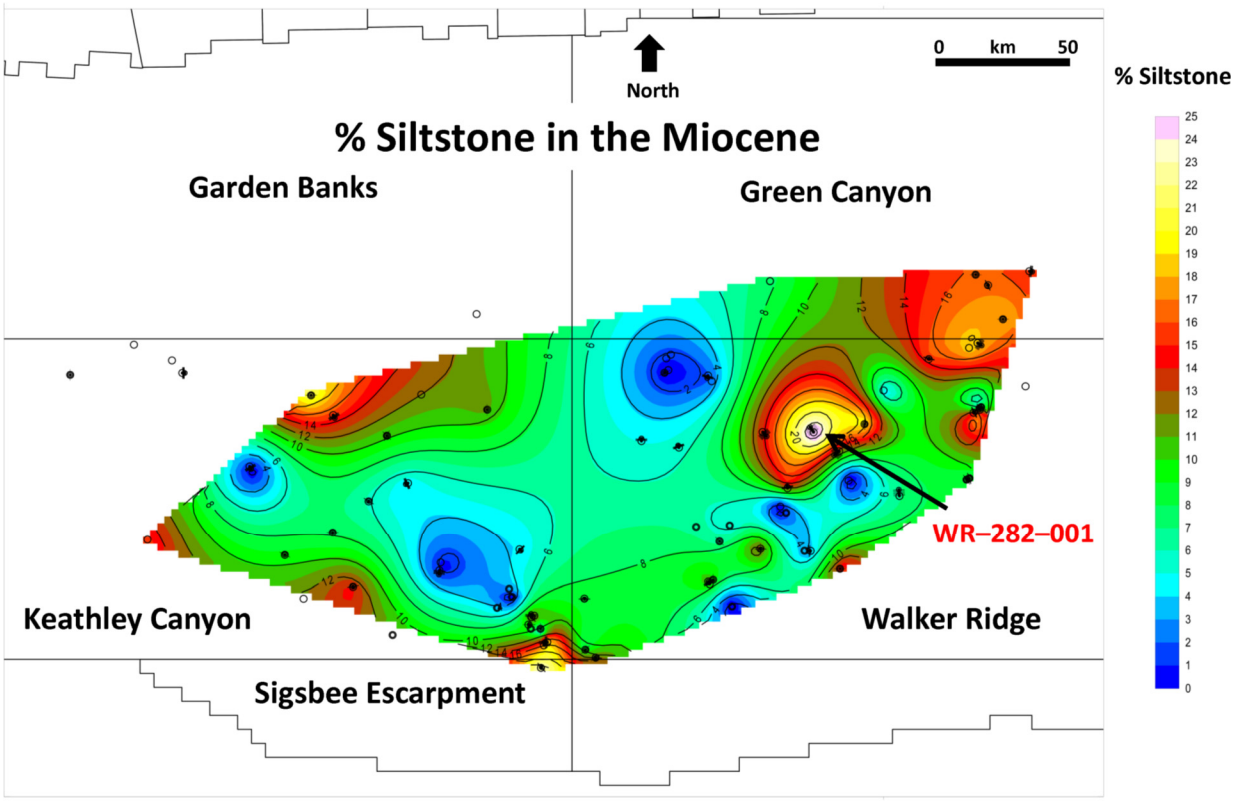

Figure 36. Map of percent (volume fraction) siltstone deposited during the Miocene Epoch. For comparison to Miocene shale percentage, please see Figure 30. 50 km = ~31 mi.

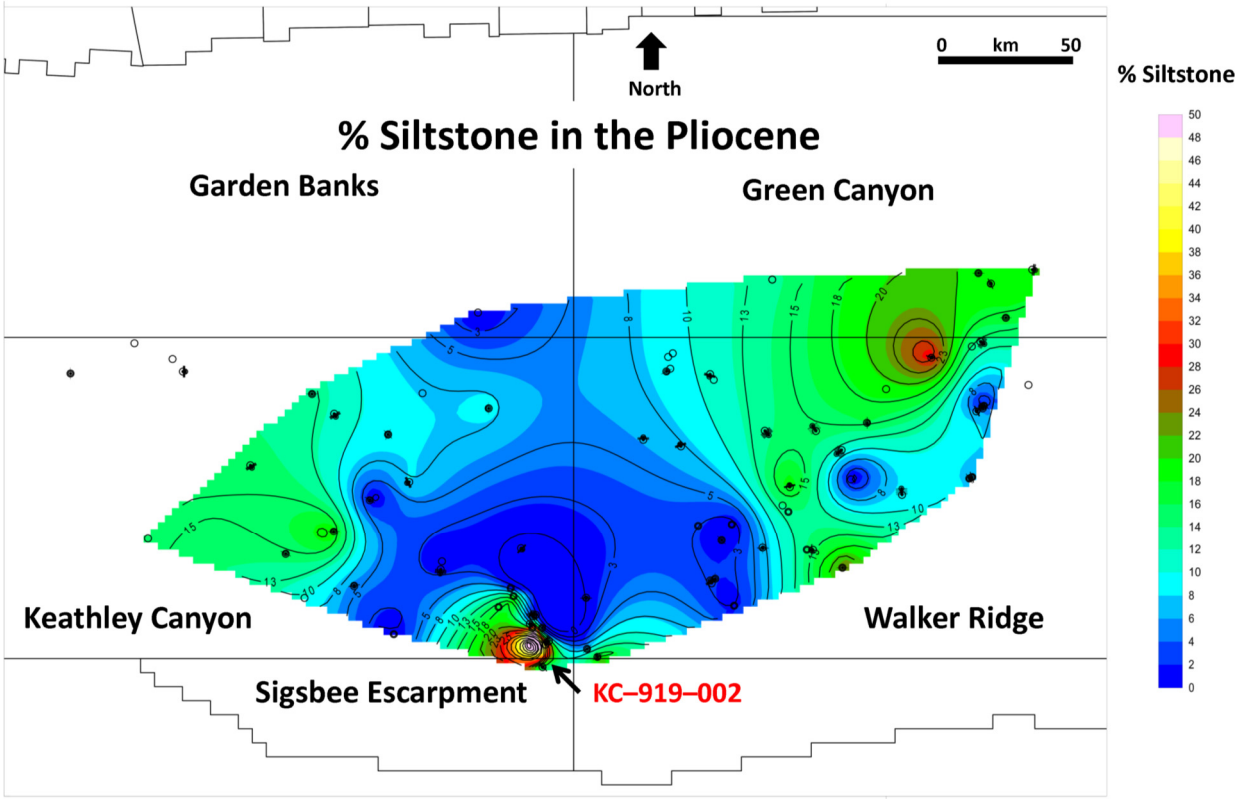

Figure 37. Map of percent (volume fraction) siltstone deposited during the Pliocene Epoch. For comparison to Pliocene shale percentage, please see Figure 31. 50 km = ~31 mi.

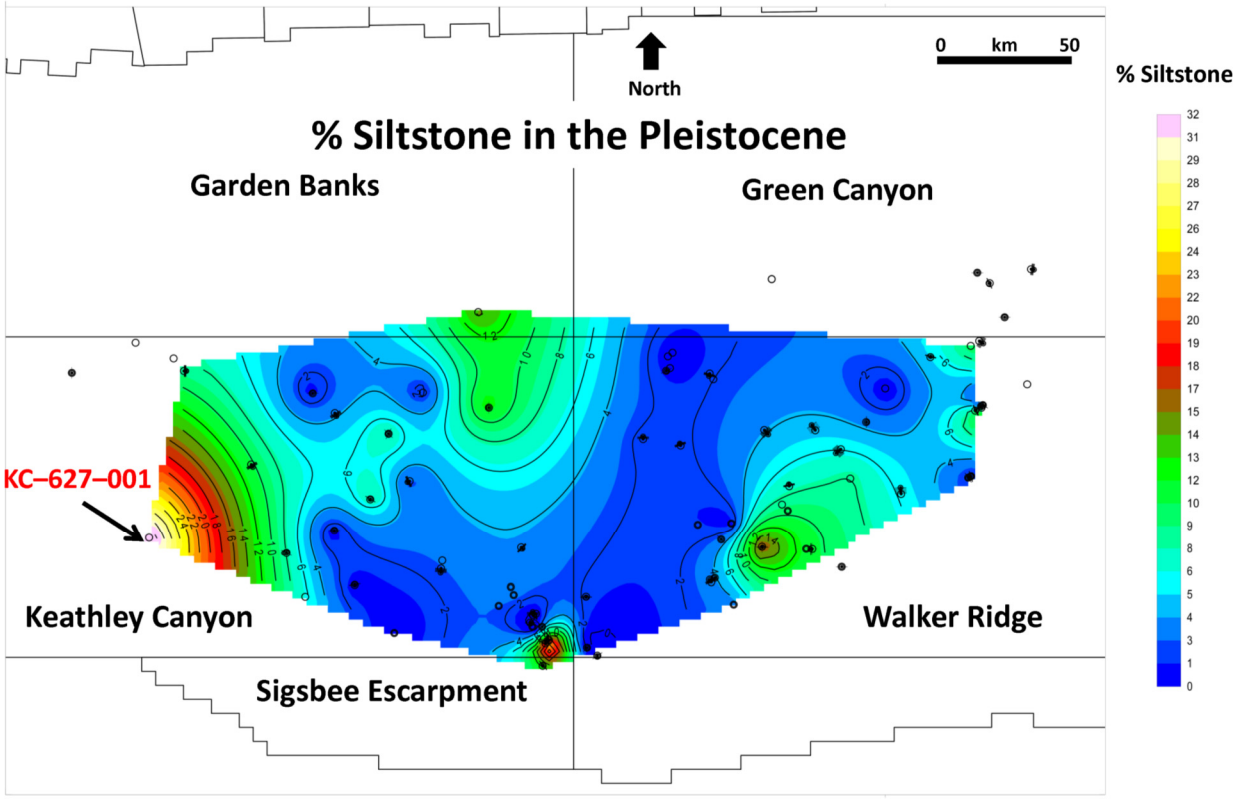

Figure 38. Map of percent (volume fraction) siltstone deposited during the Pleistocene Epoch. For comparison to Pleistocene shale percentage, please see Figure 32. 50 km = ~31 mi.

Almon, W. R., L. R. Goggin, W. C. Dawson, and F. Duque-Botero, 2009, Deepwater shale depositional systems: Seismic sedimentology: American Association of Petroleum Geologists Search and Discovery Article 90090, Tulsa, Oklahoma, 1 p., <http://www.searchanddiscovery.com/abstracts/html/2009/annual/abstracts/almon.htm> Last accessed August 21, 2018.

Bureau of Ocean Energy Management (BOEM), 2017, Assessment of technically and economically recoverable hydrocarbon resources of the Gulf of Mexico outer continental shelf as of January 1, 2014: Bureau of Ocean Energy Management OCS Report BOEM 2017–005, New Orleans, Louisiana, 43 p., <https://www.boem.gov/BOEM-2017-005/> Last accessed August 27, 2018.

Bureau of Safety and Environmental Enforcement (BSSE), 2018a, Estimated proved and unproved oil and gas reserves, Gulf of Mexico, December 31, 2006: Available in ASCII files for downloading: 2006-Tables-xls.zip, <https://www.data.bsee.gov/Main/HtmlPage.aspx?page=estimated2006> Accessed March 20, 2018.

Bureau of Safety and Environmental Enforcement (BSSE), 2018b, <https://www.bsee.gov/> Last accessed August 27, 2018.

Coleman, J., and W. E. Galloway, 1990, Petroleum geology of the Vicksburg Formation, Texas: Gulf Coast Association of Geological Societies Transactions, v. 40, p. 119–130.

Cornelius, S., and J. P. Castagna, 2018, Variation in salt-body interval velocities in the deepwater Gulf of Mexico: Keathley Canyon and Walker Ridge areas: Interpretation, v. 6, no. 1, p. T15–T27, doi:10.1190/INT-2017-0069.1.

Cornelius, S., and P. A. Emmet, 2018a, Geological 3D velocity model in Keathley Canyon and Walker Ridge, Gulf of Mexico: The Leading Edge, v. 37, no. 4, p. 299a1–299a7, doi:10.1190/tle37040299a1.1.

Cornelius, S., and P. A. Emmet, 2018b, Volume fractions of lithologic units deposited per geologic epoch in the Cenozoic, Keathley Canyon and Walker Ridge, deepwater Gulf of Mexico: Part 2—Limestone and marl: Gulf Coast Association of Geological Societies Journal, v. 7, p. 151–166, <http://gcags.org/Journal/2018.GCAGS.Journal/2018.GCAGS.Journal.v7.09.p151-166.Cornelius.and.Emmet.Part2.pdf>.

Cornish, F., 2013, Do Upper Wilcox canyons support Paleogene isolation from the Gulf of Mexico?: Gulf Coast Association of Geological Societies Transactions, v. 63, p. 183–204.

Crawford, T. G., G. L. Burgess, S. M. Haley, P. F. Harrison, C. J. Kinler, G. D. Klocek, and N. K. Shepard, 2009, Outer continental shelf: Estimated oil and gas reserves, Gulf of Mexico, December 31, 2006: Minerals Management Service, New Orleans, Louisiana, 48 p., <https://www.boem.gov/uploadedFiles/BOEM/Oil_and_Gas_Energy_Program/Resource_Evaluation/Reserves_Inventory/2009-064GOMR%281%29.pdf>, Last accessed August 27, 2018.

Dawson, W. C., and W. R. Almon, 2002, Top seal potential of Tertiary deep-water Gulf of Mexico shales: Gulf Coast Association of Geological Societies Transactions, v. 52, p. 167–176.

Dribus, J. R., M. P. A. Jackson, J. Kapoor, and M. Smith, 2008, The prize beneath the salt: Oilfield Review, August issue, p. 4–17, <https://www.slb.com/~/media/Files/resources/oilfield_review/ors08/aut08/the_prize_beneath_the_salt.pdf> Last accessed August 21, 2018.

Eikrum, V., J. Thompson, B. McKee, R. Li, J. Keller, Y. Hamilton, and G. Gray, 2011, Very large Oligocene age Frio reservoirs at Great White Field in the ultra-deepwater of the Gulf of Mexico offer significant development challenges and long-term growth potential: American Association of Petroleum Geologists Search and Discovery Article 90124, Tulsa, Oklahoma, 1 p. <http://www.searchanddiscovery.com/abstracts/html/2011/annual/abstracts/Eikrem2.html> Last accessed August 21, 2018.

Energy Information Administration (EIA), 2015, Gulf of Mexico fact sheet, <https://www.eia.gov/special/gulf_of_mexico/> Accessed March 21, 2017.

Fiduk, J. C., M. Clippard, S. Power, V. Robertson, L. Rodriguez, O. Ajose, D. Fernandez, and D. Smith, 2014, Origin, transportation, and deformation of Mesozoic carbonate rafts in the

northern Gulf of Mexico: Gulf Coast Association of Geological Societies Journal, v.3, p. 20–32, <http://gcags.org/Journal/2014.GCAGS.Journal/GCAGS.Journal.2014.vol3.p20-32.Fiduk.et.al.pdf> Last accessed August 21, 2018.

Fiduk, J. C., V. Robertson, M. Clippard, G. A. Jamieson, and S. Power, 2016, Extensional salt keels detached on the Eocene-Oligocene sediments in the deepwater northern Gulf of Mexico: Insights into canopy advancement, salt-sediment interplay, and evidence for unrecognized mass sediment displacement: Gulf Coast Association of Geological Societies Journal, v. 5, p. 47-63, <http://gcags.org/Journal/2016.GCAGS.Journal/2016.GCAGS.Journal.v5.03.p47-63.Fiduk.et.al.pdf> Last accessed August 21, 2018.

Fiduk, C., 2017, Distribution and detachment level of salt keels in deep water northern Gulf of Mexico: Insights into canopy advancement, salt sediment interplay, and evidence for unrecognized mass sediment displacement: Houston Geological Society Bulletin, v. 60, no. 2, p. 23 & 25, <https://www.hgs.org/sites/default/files/9_30_17-HGS-OctoberBulletin-final-Pages.pdf> Last accessed August 21, 2018.

Folk, R. L., 1959, Practical petrographic classification of limestones: American Association of Petroleum Geologists Bulletin, v. 43, p. 1–38.

Fort, X., and J.–P. Brun, 2012, Kinematics of regional salt flow in the northern Gulf of Mexico, *in* G. I. Alsop, S. G. Archer, and A. J. Hartley, eds., Salt tectonics, sediments and prospectivity: Geological Society of London Special Publications, v. 363, p. 265–287, doi:10.1144/SP363.12.

Fredrich, J. T., A. F. Fossum, and R. J. Hickman, 2007, Mineralogy of deepwater Gulf of Mexico salt formations and implications for constitutive behavior: Journal of Petroleum Science and Engineering, v. 57, p. 354–374.

Fulthorpe, C. S., W. E. Galloway, J. W. Snedden, P. E. Ganey-Curry, and T. L. Whiteaker, 2014, New insights into Cenozoic depositional systems of the Gulf of Mexico Basin: Gulf Coast Association of Geological Societies Transactions, v. 64, p. 119–129.

Galloway, W. E., P. Ganey-Curry, X. Li, and R. T. Buffler, 2000, Cenozoic depositional history of the Gulf of Mexico Basin: American Association of Petroleum Geologists Bulletin, v. 84, p. 1743–1774, doi:10.1306/8626C37F-173B-11D7-8645000102C1865D.

Galloway, W. E., 2008, Depositional evolution of the Gulf of Mexico sedimentary basin, *in* A.D. Miall, ed., Sedimentary basins of the world, v. 5: The sedimentary basins of the United States and Canada: Elsevier, Amsterdam, The Netherlands, p. 505–549.

Galloway, W. E., T. L. Whiteaker, and P. Ganey-Curry, 2011, History of Cenozoic North American drainage basin evolution, sediment yield, and accumulation in the Gulf of Mexico Basin: Geosphere, v. 7, p. 938–973, doi:10.1130/GES00647.1.

Hamlin, H. S., 1989, Hydrocarbon production and exploration potential of the distal Frio Formation, Texas Gulf Coast and offshore: Texas Bureau of Economic Geology Geological Circular 89–2, 47 p., <https://store.beg.utexas.edu/geologic-circulars/507-gc8902.html> Last accessed August 21, 2018.

Hudec, M. R., and M. P. A. Jackson, 2011, The salt mine: A digital atlas of salt tectonics: Texas Bureau of Economic Geology Udden Book Series 5, Austin / American Association of Petroleum Geologists Memoir 99, Tulsa, Oklahoma, p. 161–216, <https://www.aapg.org/publications/special-publications/books/details/articleid/4058/m99-the-salt-mine-a-digital-atlas-of-salt-tectonics> Last accessed August 21, 2018.

Marchand, A. M. E., G. Apps, W. Li, and J. R. Rotzien, 2015, Depositional processes and impact on reservoir quality in deepwater Paleogene reservoirs, US Gulf of Mexico: American Association of Petroleum Geologists Bulletin, v. 99, p. 1635–1648, doi:10.1306/04091514189.

McDonnell, A., R. G. Loucks, and W. E. Galloway, 2008, Paleocene to Eocene deep-water slope canyons, western Gulf of Mexico: Further insights for the provenance of deep-water offshore Wilcox Group plays: American Association of Petroleum Geologists Bulletin, v. 92, p. 1169–1189, doi:10.1306/05150808014.

Miller, K. G., M. A. Kominz, J. V. Browning, J. D. Wright, G. S. Mountain, M. E. Katz, P. J. Sugarman, B. S. Cramer, N. Christie-Blick, and S. F. Pekar, 2005, The Phanerozoic record of global sea-level change: Science, v. 310, p. 1293–1298, doi:10.1126/science.1116412.

Miller, K. G., 2009, Sea level change, last 250 million years, *in* V. Gornitz, ed., Encyclopedia of paleoclimatology and ancient environments: Springer, Dordrecht, Germany, p. 879–887, doi:10.1007/978-1-4020-4411-3_206.

Moore, D. C., H. Harrison, and F. C. Snyder, 1995, Sedimentary inclusions and internal salt stratigraphy within allochthonous salt sheets offshore Gulf of Mexico, *in* C. J. Travis, B. C. Vendeville, H. Harrison, F. J. Peel, M. R. Hudec, and B. F. Perkins, eds., Salt, sediments and hydrocarbons: Proceedings of the 16th Annual Gulf Coast Section of the Society of Economic Paleontologists and Mineralogists Foundation Research Conference, Houston, Texas, p. 193–194, <https://pubs.geoscienceworld.org/books/book/1983/chapter/11895493/sedimentary-inclusions-and-internal-salt> Last accessed August 21, 2018.

Nixon, L., E. Kazanis, and S. Alonso, 2016, Deepwater Gulf of Mexico: December 31, 2014: Bureau of Ocean Energy Management OCS Report BOEM 2016–057, New Orleans, Louisiana, 88 p., <https://www.boem.gov/Deepwater-Gulf-of-Mexico-Report-2014/> Last accessed August 21, 2018.

Rains, D. B., L. Zarra, and D. Meyer, 2007, The Lower Tertiary Wilcox trend in the deepwater Gulf of Mexico: American Association of Petroleum Geologists Search and Discovery Article 110040, Tulsa, Oklahoma, 1 p., <http://www.searchanddiscovery.com/pdfz/documents/2007/07056_62av_abs/images/ndx_rains.pdf.html> Last accessed August 21, 2018.

Rosenfeld, J. H., 2014, Paleocene-Eocene drawdown and refill of the Gulf of Mexico—Concept history and status, *in* B. Horn, N. Rosen, P. Weimer, M. Dinkleman, A. Lowrie, R. Fillon, J. Granath, and L. Kennan, eds., Sedimentary basins: Origin, depositional histories, and petroleum systems: Proceedings of the 33rd Annual Gulf Coast Section of the Society of Economic Paleontologists and Mineralogists Foundation Bob F. Perkins Research Conference, Houston, Texas, p. 330–349, <https://pubs.geoscienceworld.org/books/book/1954/chapter/11846616/paleocene-eocene-drawdown-and-refill-of-the-gulf> Last accessed August 21, 2018.

Scott, E., and A. H. Bouma, 2004, Depositional processes and reservoir characteristics of silt-stones, mudstones and shales: Society of Economic Paleontologists and Mineralogists Miscellaneous Publication, Tulsa, Oklahoma, 457 p., <https://sedimentary-geology-store.com/catalog/book/depositional-processes-and-reservoir-characteristics-siltstones-mudstones-and-shales> Last accessed August 21, 2018.

Swanson, S. M., A. W. Karlsen, and B. J. Valentine, 2013, Geologic assessment of undiscovered oil and gas resources—Oligocene Frio and Anahuac formations, United States of Gulf Coastal Plain and state waters: U.S. Geological Survey Open-File Report 2013–1257, 78 p., <https://pubs.usgs.gov/of/2013/1257/> Last accessed August 21, 2018.

Snedden, J. W., W. E. Galloway, T. L. Whiteaker, and P. E. Ganey-Curry, 2012, Eastward shift of deepwater fan axes during the Miocene in the Gulf of Mexico: Possible causes and models, Gulf Coast Association of Geological Societies Journal, v. 1, p. 131–144, <http://gcags.org/Journal/2012.GCAGS.Journal/GCAGS.Journal.2012.vol1.p131-144.Snedden.et.al.pdf> Last accessed August 21, 2018.

Snedden, J. W., W. E. Galloway, K. Milliken, and M. D. Blum, 2018, Validation of empirical source-to-sink scaling relationships in a continental-scale system: The Gulf of Mexico Basin Cenozoic record: Geosphere, v. 14, no. 2, p. 1–16, doi:10.1130/GES01452.1.

Weimer, P., 1989, Sequence stratigraphy of the Mississippi of (Plio-Pleistocene), Gulf of Mexico: Geo-Marine Letters, v. 9, no. 4, p. 185–272, <https://link.springer.com/article/10.1007/BF02431072> Last accessed August 21, 2018.

Witrock, R. B., 2017, Biostratigraphic chart of the Gulf of Mexico offshore region, Jurassic to Quaternary: Bureau of Ocean Energy Management, New Orleans, Louisiana, 1 chart, <https://www.data.boem.gov/Paleo/Files/biochart.pdf> Last accessed August 27, 2018.

Zhang, J., R. Steele, and W. Ambrose, 2017, Paleocene Wilcox cross-shelf channel-belt history and shelf-margin growth: Key to Gulf of Mexico sediment delivery: Sedimentary Geology, v. 362, p. 53–65, doi:10.1016/j.sedgeo.2017.10.001.